HHS Public Access

Author manuscript

Oncogene. Author manuscript; available in PMC 2018 October 26.

Published in final edited form as:

Oncogene. 2018 July ; 37(29): 4013–4032. doi:10.1038/s41388-018-0243-y.

Contribution of three dimensional architecture and tumor-associated fibroblasts to hepcidin regulation in breast cancer

Nicole Blanchette-Farra[1], **Daniel Kita**[2,6], **Anna Konstorum**[3], **Lia Tesfay**[1], **David Lemler**[1,7], **Poornima Hegde**[4], **Kevin P. Claffey**[2], **Frank M. Torti**[5], and **Suzy V. Torti**[1]

[1]Department of Molecular Biology and Biophysics, University of Connecticut Health Center, Farmington, CT, USA

[2]Department of Cell Biology, University of Connecticut Health Center, Farmington, CT, USA

[3]Center for Quantitative Medicine, University of Connecticut Health Center, Farmington, CT, USA

[4]Department of Pathology, University of Connecticut Health Center, Farmington, CT, USA

[5]Department of Medicine, University of Connecticut Health Center, Farmington, CT, USA

Abstract

Hepcidin is a peptide hormone that negatively regulates iron efflux and plays an important role in controlling the growth of breast tumors. In patients with breast cancer, the combined expression of hepcidin and its membrane target, ferroportin, predict disease outcome. However, mechanisms that control hepcidin expression in breast cancer cells remain largely unknown. Here we use three-dimensional breast cancer spheroids derived from cell lines and breast cancer patients to probe mechanisms of hepcidin regulation in breast cancer. We observe that the extent of hepcidin induction and pathways of its regulation are markedly changed in breast cancer cells grown in three dimensions. In monolayer culture, BMPs, particularly BMP6, regulate hepcidin transcription. When breast cancer cells are grown as spheroids, there is a >10 fold induction in hepcidin transcripts. Microarray analysis combined with knockdown experiments reveal that GDF-15 is the primary mediator of this change. The increase in hepcidin as breast cells develop a three-dimensional architecture increases intracellular iron, as indicated by an increase in the iron storage protein ferritin. Immunohistochemical staining of human breast tumors confirms that both GDF-15 and hepcidin are expressed in breast cancer specimens. Further, levels of GDF-15 are significantly correlated with levels of hepcidin at both the mRNA and protein level in patient samples, consistent with a role for GDF-15 in control of hepcidin in human breast tumors. Inclusion of tumor-associated fibroblasts in breast cancer spheroids further induces hepcidin. This induction is mediated by fibroblast-dependent secretion of IL-6. Breast cancer cells grown as

Correspondence: Professor SV Torti, Department of Molecular Biology and Biophysics, University of Connecticut Health Center, 263 Farmington Ave., Farmington, CT 06030-3305, storti@uchc.edu.

[6]Current address: Alexion Pharmaceuticals, New Haven, CT, USA

[7]Current address: Department of Molecular Biomedical Sciences, North Carolina State University, Raleigh, NC, USA

Conflict of interest statement.

The authors declare no conflict of interest.

Supplementary Information accompanies the paper on the Oncogene website: (http://www.nature.com/onc).

spheroids are uniquely receptive to IL-6-dependent induction of hepcidin by tumor-associated fibroblasts, since IL-6 does not induce hepcidin in cells grown as monolayers. Collectively, our results suggest a new paradigm for tumor-mediated control of iron through the control of hepcidin by tumor architecture and the breast tumor microenvironment.

Keywords

iron; GDF-15; hepcidin; tumor microenvironment; tumor-associated fibroblasts; spheroids

Introduction

Enhanced acquisition and retention of iron is a hallmark of breast cancer. This metabolic alteration results from changes in proteins of iron metabolism that increase iron uptake, alter iron storage, and/or reduce iron efflux: for example, transferrin receptor 1 (TfR1), the receptor that mediates uptake of transferrin-bound iron and the major iron importer of cells, is frequently upregulated in breast cancer (1–3), as is IRP2, a master regulator of intracellular iron (4). Conversely, ferroportin, an iron efflux pump, is downregulated in breast cancer cells and patient tissues (5, 6).

Hepcidin, a peptide hormone that binds to ferroportin and triggers its degradation (7), plays an important role in breast cancer. Whereas the expression of ferroportin is down-regulated in breast cancer, expression of hepcidin is upregulated (5, 6). Hepcidin secreted by breast cancer cells binds to ferroportin and initiates ferroportin degradation, thus blocking iron efflux and increasing iron retention (5, 6). Knockdown of hepcidin in breast tumor cells inhibits growth of breast tumor xenografts, indicating that hepcidin produced by tumor cells makes an important contribution to tumor growth through an autocrine/paracrine loop (6). Further, the combined expression profile of ferroportin and hepcidin is a powerful predictor of survival after mastectomy for women with breast cancer (5). Thus, the ferroportin/hepcidin regulatory axis has significant impact on tumor growth and disease progression in breast cancer patients.

In addition to its role in breast cancer, hepcidin is involved in systemic iron homeostasis: hepcidin synthesized in the liver plays a critical role in controlling systemic iron trafficking by regulating ferroportin in intestinal cells, macrophages, and hepatocytes, and thus determining the delivery of iron to the circulation (8–10). In the liver, numerous laboratories have shown that hepcidin is controlled transcriptionally by BMPs, principally BMP6 (11, 12), as well as by inflammatory cytokines such as IL-6 that increase transcription of hepcidin through a STAT3-mediated pathway (13). In breast cancer, however, pathways of hepcidin regulation are poorly understood.

Here, we probe mechanisms of hepcidin regulation in breast tumors using both two-dimensional and, to better recapitulate tissue architecture, three-dimensional (3D) cell culture (14–18). We also include tumor-associated fibroblasts in these three dimensional structures to facilitate study of the interactions that occur between the different cell types that are constituents of the tumor microenvironment. In addition to established breast cancer cell lines, we use patient-derived cells that have been conditionally reprogrammed (19) in

order to study breast cancer epithelial cells isolated directly from patients ((20); see Materials and Methods).

We report three major new findings. First, that three-dimensional culture of breast cancer cells uncovers a novel mechanism of hepcidin regulation involving GDF-15 secreted by breast epithelial cells. Second, that IL-6 derived from tumor fibroblasts further augments hepcidin secretion from breast cancer cells, implicating the tumor stroma in hepcidin regulation. Third, that the spatial organization of tumor cells alters responses to extracellular cues and activates additional pathways of hepcidin induction. These studies suggest a new paradigm for tumor-mediated control of iron through the control of hepcidin by tumor architecture and the breast tumor microenvironment.

Results

BMPs play a major role in hepcidin induction in MCF7 breast cancer cells

To investigate pathways that control hepcidin expression in breast cancer (BC), we initially examined MCF-7 cells, a well-studied breast cancer cell line (21). We confirmed that as previously described (5), MCF-7 cells grown under conventional tissue culture conditions exhibited increased hepcidin compared to non-tumorigenic MCF-10A breast epithelial cells (Supplementary Figure 1A and B), thus modeling the increased hepcidin seen in breast cancer.

We first considered the contribution of bone morphogenetic proteins (BMPs) and interleukin 6 (IL-6) to hepcidin regulation in breast cancer cells, since these pathways regulate hepcidin transcription in the liver through activation of SMAD and STAT3 signaling pathways, respectively (11, 22). Measurement of endogenous transcript levels revealed that MCF-7 cells had higher expression of several BMPs implicated in control of hepcidin than MCF-10A cells, particularly BMPs-4, 6 and 7 (Figure 1A and Supplementary Table 1). Additionally, MCF-7 cells expressed BMP receptors required for downstream BMP signaling (Supplementary Figure 1C). To directly test the role of BMPs in hepcidin regulation, we depleted endogenous BMPs with siRNA and assessed the effect on hepcidin. Knockdown of BMPs was efficient (60–95%) (Supplementary Figure 1 D–F). Although depletion of all three BMPs reduced hepcidin (Figure 1B), knockdown of BMP6 resulted in a more pronounced decrease in hepcidin than knockdown of BMP4 or BMP7 (Figure 1B). Antibodies directed at BMPs were also effective at reducing hepcidin, particularly anti-BMP-6 and anti-BMP4 (Figure 1C). We next investigated the role of IL-6 and the STAT3 signal transduction pathway in regulation of hepcidin in MCF7 cells. Although IL-6 transcripts were non-detectable (Supplementary Table 1), MCF-7 cells expressed IL-6 receptor (Supplementary Figure 1C). Further, alternative activators of STAT3 signaling such as IL-1, IL-5, interferons or epidermal growth factor (EGF) have been described (23–26), and it was possible that these might trigger STAT3 activation and increase hepcidin synthesis. We therefore treated MCF-7 cells with recombinant IL-6 and measured effects on activation of STAT3 and hepcidin. Although STAT3 was successfully activated by IL-6 under these conditions, there was no corresponding induction of hepcidin (Figure 1D). Taken together, these results suggest that among previously identified regulators of hepcidin, BMPs, particularly BMP6, play a predominant role in MCF-7 breast cancer cells.

Hepcidin is dramatically induced in breast cancer spheroids

Recent results have suggested that three-dimensional (3D) culture may be useful for studying metabolic changes in cancer, particularly breast cancer (27, 28). To test whether additional pathways regulating hepcidin might be uncovered using three-dimensional culture, we grew MCF-7 breast cancer cells and the non-tumorigenic MCF-10A breast cell line as three-dimensional spheroids. Cells were plated in wells coated with poly(2-hydroxy-ethyl methacrylate)(polyHEMA), which prevents cell adhesion and fosters the spontaneous aggregation of cells into multicellular spheroids, as previously described (29). As shown in Figure 2A, under these conditions both MCF-10A non-tumor and MCF-7 tumor cells formed viable spheroids as demonstrated by calcein-AM staining (Figure 2A).

We measured hepcidin levels in MCF-10A and MCF-7 cells grown under these 3D culture conditions and compared them to hepcidin synthesized by cells grown in monolayers. As expected, hepcidin expression was increased in MCF-7 spheroids when compared to MCF-10A spheroids (Figure 2B and E). Strikingly, when levels of expression of hepcidin in cells grown under two and three dimensional culture conditions were compared, there was a 15 fold increase in hepcidin mRNA and 2–3 fold induction of hepcidin protein in MCF-7 cells grown in 3D (Figure 2C and F). This difference was not seen in MCF-10A cells, which exhibited similar levels of hepcidin under both two and three dimensional culture conditions (Figure 2D and G). Normal mammary epithelial cells (HME) similarly exhibited no increase in hepcidin when grown under 3D culture conditions (Supplementary Figure 1G). To ensure that the difference in hepcidin expression between 2D and 3D was not a consequence of altered rates of proliferation of cells grown under these two different culture conditions, we examined hepcidin expression at later time points, when proliferative rates, as measured by Ki67 gene expression (30), were similar between cells grown in 2D and 3D (Supplementary Figure 1H). We found that hepcidin induction was preserved under these conditions (Supplementary Figure 1H), suggesting that the 3D environment, rather than the rate of proliferation, underlies hepcidin induction in spheroids.

Hepcidin is induced in breast cancer spheroids prepared from patient cells

To confirm the selective induction of hepcidin in breast cancer spheroids, we next turned to primary breast epithelial cells. Breast cancer cells were isolated directly from breast tumors. At the same time, non-malignant breast epithelial cells were obtained from normal adjacent tissue to serve as patient-matched controls. Both malignant and non-malignant epithelial cells were expanded on irradiated fibroblast feeder layers and re-plated in the absence of feeder layers prior to initiating experiments (detailed methodology is provided in Materials and Methods (20)). Cells exhibited typical epithelial markers, including E-cadherin and pan-cytokeratin (Supplementary Figure 2A and B). Vimentin, a mesenchymal marker, was not expressed (Supplementary Figure 2A). Tumor cells expressed higher levels of N-cadherin (31), a protein associated with breast cancer cell motility and invasion, than non-cancer epithelial cells isolated from the same patient (Supplementary Figure 2A).

We then measured hepcidin levels in these patient-derived normal and tumor cells. Tumor cells expressed increased levels of hepcidin transcripts when compared to normal cells under both monolayer and 3D culture conditions (Supplementary Figure 2C and D). As we had

observed in MCF-10A and MCF-7 cells, the difference in hepcidin expression was particularly pronounced in cells grown as spheroids. We also examined the expression of hepcidin using immunofluorescent staining. Consistent with changes observed at the mRNA level, there was a substantial increase in hepcidin in tumor cells (Figure 3A). This was accompanied by a decrease in ferroportin in tumor spheroids compared to spheroids from normal cells (Figure 3A), suggesting that hepcidin produced by spheroids is functional in targeting ferroportin for degradation. To confirm the functionality of hepcidin in breast tumor spheroids, we treated cells with two different anti-hepcidin antibodies and assessed the consequences of this treatment on levels of ferroportin. As expected, blockade of hepcidin by anti-hepcidin antibodies increased ferroportin, indicating that hepcidin synthesized by these cells functions in an autocrine fashion and exerts its expected biological activity (Figure 3B).

Next, we compared the effects of 3D culture on hepcidin in breast cancer and normal cells. Using primary breast tumor spheroids derived from four separate breast cancer patients (Table 1), we observed a marked hepcidin induction in 3D culture compared to 2D (Figure 3C and Supplementary Figure 2E–H), with increases in transcript levels ranging from 10 to 22 fold. In contrast to MCF10A cells, which did not increase synthesis of hepcidin when cultured in 3D (Figure 2D and G), hepcidin was also induced in spheroids from normal cells, albeit at lower levels than in tumor cells (~3.5 fold transcriptionally) (Figure 3C).

To assess whether the increase in hepcidin observed in 3D cultures of tumor cells was associated with changes in intracellular iron, we measured levels of ferritin. Ferritin is an iron storage protein composed of H and L subunit types (32). Because levels of ferritin are post-transcriptionally increased by iron (33–35), it is frequently used as a surrogate marker for intracellular iron. We anticipated that increased hepcidin would lead to decreased ferroportin, thus reducing iron efflux and increasing intracellular iron and ferritin. As shown in Figure 3D, expression of both ferritin H and L subunits was indeed increased from 2D to 3D culture in patient tumor cells, suggesting that the increased levels of hepcidin seen in tumor spheroids contributes to a phenotype of iron retention.

BMPs and IL-6 make modest contributions to hepcidin induction in breast cancer spheroids

We next sought to determine the regulatory pathways responsible for hepcidin induction in breast cancer spheroids. As seen with monolayer cells, measurement of transcript levels revealed that BMPs, particularly BMP-4, 6 and 7, were basally expressed in MCF-7 spheroids and expression was increased compared to MCF-10A spheroids (Supplementary Figure 3A–D). Additionally, MCF-7 spheroids expressed BMP receptors, and BMP receptor expression was enhanced in 3D culture compared to monolayer culture (Supplementary Figure 3E). In contrast, and consistent with monolayer cells, expression of IL-6 was not observed in MCF-7 spheroids (Supplementary Figure 3D).

To test the contribution of BMPs and IL-6 in regulation of hepcidin synthesis in spheroids, we first reduced levels of endogenous BMPs 4, 6 and 7 using siRNA (Supplementary Figure 3F–H) and assessed effects on hepcidin expression. Depletion of BMPs reduced hepcidin expression in MCF-7 spheroids (Figure 4A and 4B); depletion of BMP6 had the most

pronounced effect, resulting in an approximate reduction of 30–35% in hepcidin transcripts and 20% reduction in hepcidin protein compared to non-targeting control (NTC). Similar to what we had observed in 2D, there was no detectable expression of IL-6 and minimal phosphorylation of STAT3 in MCF-7 spheroids (Figure 4C), and knockdown of STAT3 using siRNA only modestly reduced hepcidin transcripts (~20%) (Figure 4D).

Growth Differentiation Factor 15 (GDF-15) induces hepcidin expression in BC spheroids

Since none of the classical regulators of hepcidin explained the 10–22 fold transcriptional increase in hepcidin expression seen in spheroids (Figure 2C and Supplementary Figure 2E–H), we next examined differences in global gene expression between MCF-7 cells grown as monolayers and spheroids to search for non-canonical mechanisms that might underlie the induction of hepcidin in spheroids. To assure that differences we observed were independent of the specific method used to induce spheroid formation, we compared gene expression profiles from cells grown using three different methods of 3D culture: spheroids cultured in polyHEMA-coated 96-well plates; spheroids cultured in ultra-low attachment 96-well plates; and spheroids cultured in 0.24% methylcellulose (36). Hepcidin was upregulated to a similar extent using all three of these methods when compared to monolayer culture (Supplementary Figure 4A).

Overall, from 1809 to 2117 genes were significantly differentially expressed in MCF-7 spheroids, depending on the 3D culture condition (Supplementary Table 2). Specific gene expression changes observed between 2D and 3D were remarkably similar using each of the 3 methods of 3D cell culture (Table 2). GAGE Pathway analysis revealed that global differences in gene expression profiles induced by 3D culture were similar to those previously described, including cell cycle, DNA replication and mismatch repair (Table 3) (37–39). Nine of the top 10 perturbed pathways were the same in all three 3D cases, although there were differences in their rank order (Table 3).

To search for inducers of hepcidin, we examined genes that were most significantly upregulated under all three 3D culture conditions (Table 2). Notable among these was GDF-15: induction of GDF-15 ranged from 16.07 to 21.9 fold (FDR p-value $p<0.009$) (Table 2). Expression (Bi-weight average signal (log2)) of GDF-15 was robust, with an average expression level roughly equivalent to the mean of all other genes expressed in these cells (Supplementary Figure 4B–D).

Growth differentiation factor-15 (GDF-15), also called MIC-1 (40), is a member of the TGF-β superfamily that is up regulated in many cancers, including breast cancer (40, 41). GDF-15 has previously been shown to correlate with and potentially regulate hepcidin, although in some contexts GDF-15 may act as an inhibitor rather than an activator of hepcidin (see Discussion and (42–45)). We observed that GDF-15 was increased in our breast cancer cell models when compared to non-cancer cells: MCF-7 spheroids had increased GDF-15 compared to MCF-10A spheroids, as did patient tumor spheroids compared to spheroids derived from normal adjacent cells (Figure 5A and B). To confirm the induction of GDF-15 seen in the microarray analysis, we measured GDF-15 mRNA using qRT-PCR and GDF-15 protein using an ELISA assay in MCF-7 cells grown as monolayers or spheroids. As anticipated, MCF-7 spheroids exhibited increased GDF-15

expression (transcript and protein) relative to monolayer cultures (Figure 5C and D). Increased expression of GDF-15 was correlated with increased hepcidin expression in 3D spheroids (Figure 5E and F). To confirm the generality of these findings, we also examined GDF-15 in patient-derived breast cancer cells. Similar to MCF-7 cells, primary tumor cells also exhibited a pattern of increased GDF-15 expression from 2D to 3D culture (Supplementary Figure 5A and 5B).

To directly test whether GDF-15 induced hepcidin, we used siRNA to reduce levels of GDF-15 in BC spheroids. We observed that efficient knock-down of GDF-15 (~85%; Supplementary Figure 5C and D) significantly reduced hepcidin expression at both the transcript and protein levels (~70% and 50% respectively) (Figure 6A and B and supplementary Figure 5E). Although GDF15 knockdown did not completely abrogate the induction of hepcidin seen in spheroids (Figure 6A), reducing GDF-15 had a greater inhibitory effect than blocking either BMP6 or STAT3 (Figure 4).

GDF15-dependent hepcidin induction in spheroids is mediated by SMAD1-5-8

Our next goal was to assess the signaling pathway linking GDF-15 to hepcidin production. Although GDF-15 downstream signaling is incompletely understood, there is evidence that GDF-15 may utilize the SMAD pathway (46, 47). SMAD signaling proceeds via two divergent pathways: pSMAD2-3 (TGFβ signaling) and pSMAD1-5-8 (BMP signaling) (48). We assessed the activity of both these pathways in 2D versus 3D culture using a western blot for activated (phosphorylated) SMAD2-3 and SMAD1-5-8. As shown in Figure 6C, only SMAD1-5-8 was activated from 2D to 3D culture of MCF-7 cells. Further, reduction of GDF-15 in MCF-7 spheroids using siRNA simultaneously reduced SMAD1-5-8 activity (Figure 6D) and hepcidin synthesis (Figure 6A), both of which were restored by addition of recombinant GDF-15 (Supplementary Figure 5F–H).

Our 3D results prompted us to examine a role for GDF-15 in control of hepcidin in 2D. As shown in Figure 6, hepcidin levels did not change following either knockdown of GDF-15 (Figure 6E and F and Supplementary Figure 6A–D) or addition of exogenous GDF-15 at concentrations ranging from the sub- to the supra-physiological (Supplementary Figure 6E) in 2D cultures. Together, these data suggest that GDF-15 regulates hepcidin induction breast cancer spheroids selectively, and does so through the activation of a SMAD1-5-8-dependent pathway.

Expression of GDF-15 and hepcidin are correlated in breast cancer tissue

To test whether an association between GDF-15 and hepcidin was also present in breast cancer tissue, we first analyzed hepcidin (gene symbol *HAMP*) and GDF-15 (gene symbol *GDF15*) transcripts in the publicly available TCGA breast cancer dataset (49). Levels of both transcripts were significantly increased in cancer tissue (n=526) compared to normal adjacent tissue (n= 61) ($p<6\times10^{-7}$ for *GDF15*, $p<0.0003$ for *HAMP*) (Figure 7A and B). We divided tumors into two groups based on hepcidin expression (above or below the mean) and assessed *GDF15* expression in these two groups. *GDF15* expression was significantly different among the high and low subdivisions of *HAMP* ($p<0.01$), with high *HAMP* associated with high *GDF-15* expression (Figure 7C). Similarly, when tumors were divided

into two groups based on *GDF15* expression, high *GDF15* was significantly associated with high *HAMP* ($p<0.04$) (Figure 7D).

To explore the relationship between GDF-15 and hepcidin at the protein level and to assess whether both proteins were expressed in breast epithelial cells, we performed immunohistochemical analysis of tumor sections from 56 breast cancer patients. As shown in Figure 7E, expression of both GDF-15 and hepcidin was evident in breast cancer tissue. Staining with pan-cytokeratin confirmed the expression of both proteins in epithelial cells. Expression of GDF-15 and hepcidin were also faintly evident in some surrounding stromal cells (Figure 7E). Further, as illustrated in Figure 7E and quantified in Figure 7F, there was a strong positive correlation between GDF-15 and hepcidin in epithelial cells ($R^2=0.44$, $p<3\times10^{-8}$), consistent with a role for GDF-15 in regulation of hepcidin in human breast tumors *in vivo*.

Tumor Associated Fibroblasts Contribute to hepcidin induction via paracrine IL-6 signaling

In addition to autocrine regulation of hepcidin by tumor epithelial cells themselves, we asked whether other cell types in the tumor microenvironment might contribute to hepcidin induction. In particular, we focused on tumor associated fibroblasts (TAFs), since these cells are known to support tumor growth through secretion of pro-inflammatory cytokines and growth factors (50). TAFs isolated from patient tumor tissue were fibroblastic in shape and expressed vimentin, a mesenchymal marker (Supplementary Figure 7A). When TAFs were co-cultured with tumor epithelial cells (TECs), we observed a significant increase in hepcidin (Figure 8A and B).

We then explored the mechanism of TAF-dependent induction of hepcidin. To test whether the induction of hepcidin by TAFs required direct cell contact or was mediated by a secreted factor, we prepared conditioned medium from TAFs and cultured TEC spheroids in this medium. As shown in Figure 8C, an increase in hepcidin was detected when TEC spheroids were exposed to conditioned media (CM) from TAFs, supporting the role of a secreted factor in hepcidin induction. We then measured levels of known hepcidin agonists in TAFs. We found that TAFs produced copious IL-6, with no detectable levels of BMP6 or GDF-15 (Supplementary Figure 7B). Additionally, primary tumor epithelial cell (TEC) spheroids expressed IL-6 receptor (IL-6R), suggesting their potential ability to respond to paracrine IL-6 signaling (Supplementary Figure 7C).

We therefore tested whether the TAF factor that induced hepcidin was IL-6. TEC were cultured in the presence of either TAFs or TAF CM. pSTAT3, the downstream signal activator of IL-6, was then measured. As shown in Figure 8D, both TAFs and TAF conditioned medium activated STAT3. We then directly evaluated the role of IL-6 in stimulating hepcidin by incubating the conditioned medium with neutralizing anti-IL-6 antibody before addition to TEC spheroid culture. We found that depletion of IL-6 from CM (Supplementary Figure 7D) significantly reduced hepcidin levels (Figure 8E and F). Consistent with these results, the addition of recombinant IL-6 to TEC cultures stimulated hepcidin synthesis (Supplementary Figure 7E and F). These results suggest that TAFs in the tumor microenvironment contribute to the synthesis of hepcidin in breast cancer epithelial

cells through secretion of IL-6. A model of hepcidin regulation in breast cancer is shown in Figure 9.

Discussion

The significant association between iron efflux pathways and breast cancer patient outcome (5), as well as the role of hepcidin in breast tumors *in vivo* (6) prompted us to investigate mechanisms of hepcidin control in breast cancer. We used 3D culture of both breast cancer cell lines and patient-derived breast tumor cells to more fully explore mechanisms controlling hepcidin synthesis *in vivo*.

Three dimensional culture is an important tool in the study of breast cancer growth and metabolism that can provide unique biological insights not evident in cells grown in 2D (17). It has been suggested that 3D culture may more successfully predict tumor cell behavior *in vivo* than 2D models, since breast cancer cells grown in 3D exhibit a gene expression profile that more closely mimics human tumors than cells grown in 2D (51, 52). 3D culture is a promising tool for drug screening that may more accurately predict clinical success of anti-cancer drugs (53, 54). In the present study, we found that BMPs, particularly BMP6, were important regulators of hepcidin synthesis in breast cancer cells grown in both 2D and 3D (Figure 1 B and C and Figure 4 A and B). However the growth of breast cells in 3D allowed additional regulatory mechanisms to become evident.

The first novel pathway of hepcidin regulation that we observed in cells grown in 3D was mediated by GDF-15. GDF-15 is a member of the TGF-β superfamily that plays a broad role in tissue homeostasis and repair (40). GDF-15 is induced in response to inflammation, acute injury or malignancy (41, 55, 56). Serum levels of both GDF-15 and hepcidin are increased in patients with breast cancer (6, 41) and other malignancies (42, 43, 57). GDF-15 may play multiple roles in cancer; however, studies in breast cancer cells have suggested a role of GDF-15 in enhanced invasion as well as in maintenance of breast cancer stem cells (58, 59). We observed that GDF-15 and hepcidin mRNA were both elevated in primary cells from breast tumor tissue compared to normal adjacent tissue (Figure 3 and Figure 5). Further, immunohistochemical staining of breast cancer tissue arrays (Figure 7E) as well as interrogation of publicly available microarray datasets from breast cancer patients (Figure 7 A–D) indicated that there was a positive correlation between GDF-15 and hepcidin in breast tissue. Our work thus extends the known functions of GDF-15 to the local regulation of hepcidin in tumor tissue, representing a new role for GDF-15 in tumorigenesis. Specifically, the upregulation of GDF-15 and consequent increase in hepcidin in tumor tissue may foster tumor growth by enhancing tumor iron retention. The increase in ferritin we observed in tumor spheroids (Figure 3) is consistent with this interpretation.

GDF-15 has previously been described as a negative regulator of hepcidin, since high serum levels of GDF-15 in patients with β-thalassemia were associated with suppression of hepatic hepcidin (44). However, in this same study, the response of hepatocyte cells to GDF-15 in vitro was shown to be biphasic, with lower levels of GDF-15 stimulating hepcidin synthesis, and higher levels (≥ 10,000 pg/ml) inhibiting hepcidin (44). We observed that the level of

GDF-15 produced by breast cancer spheroids ranged from 100–500 pg/ml, consistent with an inductive effect of GDF-15 on hepcidin.

GDF-15 and the BMPs are both members of the TGF-β superfamily. Previous work has identified SMAD1-5-8 as the regulatory pathway that mediates induction of hepcidin by BMPs in hepatocytes (60). Although the receptor(s) and signaling pathways activated by GDF-15 have been less well studied than those that mediate BMP activity, experiments presented here suggest that GDF-15 may also utilize a SMAD1-5-8 signaling pathway to control hepcidin induction in spheroids. Further supporting this, both hepcidin and activated SMAD1-5-8 were abrogated when GDF-15 was decreased with siRNA in spheroids (Figure 6) and this effect was rescued with the addition of recombinant GDF-15 (Supplementary Figure 5). Hepcidin regulation by GDF-15 seems specific to spheroids, as treatment of MCF-7 monolayers with GDF-15 had no effect on hepcidin expression (Supplementary Figure 6). Although we did not study the mechanism underlying the activation of a GDF-15-mediated regulatory pathway in spheroids, it is well known that metabolic pathways, intercellular communication, and signaling all differ significantly in cells grown in 3D versus 2D (14, 39, 61). In our experiments, we observed an increase in activated SMAD1-5-8 in spheroids (Figure 6C), which may contribute to the elevated hepcidin levels observed in 3D cultures. Further work will be required to elucidate mechanisms underlying the induction of a GDF-15-mediated hepcidin regulatory pathway in spheroids.

The second major observation to emerge from this study is that stromal cells in the tumor microenvironment can contribute to regulation of hepcidin synthesis in breast tumor cells. Stromal cells play a significant role in breast tumorigenesis and secrete factors such as TGF-β and IGF-1 that can directly activate pathways in tumor epithelial cells (TECs)(50) (reviewed in (50, 62)). For example, TAFs have been found to secrete CXCL12 for promotion of proliferation, migration and invasion of breast tumor epithelial cells (63). We found that IL6 secreted by TAFs significantly contributes to hepcidin synthesis (Figure 8). TAFs grown in the absence of TECs showed minimal hepcidin expression (Figure 8A and B), suggesting that co-culture induces hepcidin primarily in TECs rather than in the TAFs themselves. Consistent with this interpretation, conditioned media from TAFs induced hepcidin in TECs to a similar extent as co-culture with TAF cells (Figure 8C).

Since IL-6 was the only ligand previously associated with induction of hepcidin that was produced by TAFs, and TAF-mediated induction of hepcidin could be blocked by anti-IL-6 antibody (Figure 8), our experiments suggest that IL-6 is the major and perhaps only factor secreted by TAFs that influences hepcidin synthesis. However a limitation of our studies is that we were unable to isolate TAFs from multiple patient samples. In addition, multiple additional cell types populate the tumor microenvironment, including immune cells of several lineages (64), and these have been implicated in modifying local iron homeostasis in breast tumors (65). Thus, more extensive analyses are likely to uncover additional regulators that contribute to fine-tuning hepcidin synthesis in the tumor microenvironment. Interestingly, although we did not observe secretion of GDF-15 in breast cancer TAFs (Supplementary Figure 7B), GDF-15 is secreted by TAFs isolated from prostate tumors and promotes prostate tumorigenesis (66). Since hepcidin is also upregulated in prostate tumors

(67), it is possible that in prostate cancer, TAFs may contribute to hepcidin synthesis through secretion of GDF-15.

A third observation to emerge from our studies is that an alteration in the spatial configuration of tumor cells is sufficient to alter responses to extracellular cues and activate additional pathways of hepcidin induction. Thus, although cells grown in 2D displayed receptors rendering them potentially responsive to IL-6, hepcidin synthesis was not triggered by treatment with exogenous IL-6 in cells grown in 2D (Figure 1D). In contrast, breast cancer cells grown in 3D induced hepcidin when exposed to IL-6 (Figure 8 and Supplementary Figure 7 E and F). This result underscores the importance of spatial organization in the activation of tumor signaling pathways, including those that regulate iron metabolism.

Mechanisms of regulation we observed in cell lines were recapitulated in cells derived from patient tissues (Figure 3 and Supplementary Figures 2, 5). However, a limitation of our study is that the patient-derived cells we examined were all derived from tumors that were hormone receptor (HR) positive, HER2 negative -- i.e., all expressed estrogen receptor (ER) and all were negative for HER2, important prognostic markers in breast cancer. Although the $HR^{+}HER2^{-}$ phenotype is representative of the majority of breast tumors (68), it does not capture the full spectrum of breast cancers, which have recently been divided into at least 5 molecular subtypes with significantly different clinical outcome (69, 70). It will be of interest to determine whether molecular subtype influences hepcidin regulation, particularly since our previous microarray analyses have shown that hepcidin is associated with poorer patient outcome in tumors that express high levels of ferroportin (5).

Collectively, the experiments presented here demonstrate the existence of multiple mechanisms that coordinately control hepcidin synthesis in breast tumor spheroids. Studies of mechanisms through which tumor cells and cells in the tumor microenvironment regulate synthesis of hepcidin may not only uncover new pathways through which hepcidin is controlled, but may ultimately suggest new strategies for inhibiting local synthesis of hepcidin that can be used to target the metabolic dependence of tumor cells on iron.

Materials and Methods

Cell Line Culture

MCF-7 and MCF-10A cells were obtained from the Wake Forest University Comprehensive Cancer Center Tissue Culture Core facility and verified by ATCC cell authentication testing service. HME cells were purchased from Lonza (Basel, Switzerland). MCF-7 cells were cultured in Dulbecco's minimal essential medium (DMEM)–F12 (Thermo Fischer Scientific, Waltham, MA, USA) supplemented with 10% FBS (Gemini Bio-Products, West Sacramento, CA, USA). MCF-10A and HME cells were cultured in Mammary Epithelial Growth medium (MEGM) bullet kit (Lonza; catalog #CC-3150). MCF-10A media was supplemented with 100μg/ml cholera toxin (Sigma-Aldrich, St. Louis, MO, USA). All cells were maintained at 37°C in a humidified atmosphere containing 5% CO2 and 20% O2.

Patient Sample Isolation

De-identified tumor and adjacent non-tumor human mammary tissue was obtained under the approval of the Institutional Review Board of University of Connecticut Health. Fresh specimens were put into F media (19) [3:1 v/v Ham's F12 Nutrient Mix: Dulbecco's Modified Eagle Medium (Thermo Fischer Scientific), 5% fetal bovine serum (Gemini Bio-Products, West Sacramento, CA, USA), 0.4 μg/mL hydrocortisone (Sigma-Aldrich), 5 μg/mL recombinant human insulin (Life Technologies, Carlsbad, CA), 8.4 ng/mL cholera toxin (Sigma-Aldrich), 10 ng/mL epidermal growth factor (EMD Millipore, Billerica, MA, USA), 24 μg/mL adenine (Sigma-Aldrich), penicillin-streptomycin (Life Technologies), and 10 μmol/L Y-27632 (Tocris Bioscience, Bristol, United Kingdom)], and placed immediately on ice.

Primary Cell Culture

Primary cell culture was performed using a conditional reprogramming technique as previously described (20). Briefly, specimens were removed of excess fat, minced, and then digested in 0.1 U/mL collagenase and 0.8 U/mL dispase (Roche Diagnostics, Indianapolis, IN, USA) for approximately 1–2 hrs at 37°C. The cell suspension was passed through a 100 μm nylon filter and centrifuged at 400 × g. The cell pellet was re-suspended in F media and washed three more times to ensure removal of the proteases. For tumor associated fibroblast (TAF) culture propagation (from patient 113), half of the re-suspended cell pellet was directly plated in dishes overnight in F-media and re-fed the next day with F-media minus cholera toxin. TAFs were cultured in a 37°C humidified incubator with 5% CO2 and 7% O2. Expanded cells were trypsinized with 0.05% trypsin and re-plated up to five passages before freezing as stocks. For tumor/adjacent normal epithelial cells, the remaining re-suspended cell pellet was plated onto irradiated (4000 Rad) mouse NIH 3T3 fibroblasts in the presence of 10 μmol/L Y-27632 (Tocris) and cultured in F-media at 37°C humidified incubator with 5% CO2 and 7% O2. Cells were passaged by differential trypsinization; when approximately 90% confluent, the cells were incubated with 0.05% trypsin to first remove the feeder fibroblast cells. The detached fibroblasts were aspirated and the remaining epithelial cells were incubated with 0.25% trypsin until detached. The cells were neutralized with equal volume F media, re-suspended gently to generate a single cell suspension, and centrifuged at 400 × g. The cells were re-suspended in F media and passaged at 1:2 – 1:4 ratios onto irradiated feeder cultures. NIH 3T3 fibroblasts were maintained in DMEM (Thermo Fischer Scientific) supplemented with 10% FBS (Gemini Bio-Products) and 1% Pen-Step for initial culturing before use as a feeder layer. For use in all experiments, primary cells were passaged directly from conditional reprogrammed conditions and plated as monolayers or spheroids without 3T3 fibroblasts in F-media without Y-27632 to re-differentiate cells for at least 2 days.

Spheroid Culture

24 hours before spheroid plating, U-bottom 96-Well Polystyrene Round Bottom Microwell Plates (Thermo Fischer Scientific) were coated with Poly(2-hydroxyethyl methacrylate) (polyHEMA) (Sigma-Aldrich). Briefly, 2.4g of polyHEMA was dissolved in 20mL of 70% EtOH to make a 10X stock. A 1X solution was prepared with 70% EtOH and 30ul per well

was added. Plates were left in laminar flow hood overnight to ensure EtOH evaporation. To generate spheroids, cells were trypsinized from monolayer cultures and cells were seeded at 8,000 cells/well in polyHEMA coated plates in corresponding normal growth media. In some experiments, spheroids were plated in basal growth media containing no serum. To examine spheroid viability, 2uM calcein-AM (Life Technologies) was added to spheroid wells and live spheroids were imaged using a fluorescent inverted microscope (Zeiss Axio Vert.A1; Carl Zeiss Microscopy, Jena, Germany). For microarray analysis only, additional spheroid techniques were used, including plating 8,000 cells in ultra-low attachment 96-well plates (Corning INC, Corning, NY, USA) or the addition of methylcellulose (Sigma-Aldrich) (0.24% total) as an aggregating agent, as previously described by Longati et al. (36).

Tumor Associated Fibroblast (TAF) and Tumor Epithelial Cell (TEC) Co-Culture and Conditioned Media Treatments

Tumor associated fibroblasts from patient 113 (TAFs) were propagated in F-media. For conditioned media (CM) experiments, 90% confluent cultures were replenished with fresh F-media and allowed to secrete for 48 hours before removal of CM and subsequent addition of CM to TEC cultures (8000 cells/spheroid). For direct co-cultures, TECs were trypsinized and TAFs were trypsinized and irradiated (4000 rad). For co-culture spheroid generation, co-cultures were produced by mixing 80% TEC/20% TAF (6400 cells/1600cells) or 100% TEC/20% TAF (8000/1600) in F-media immediately before plating as spheroids.

Neutralizing antibody and recombinant protein treatments

For neutralization of BMPs, cells were treated with 1 or 3 μg/mL anti-BMP4, anti-BMP6, anti-BMP7, (R&D Systems, Minneapolis, MN, USA cat#MAB757, MAB507, MAB3541) or 3 μg/mL isotope-matched anti-IgG (R&D systems, cat#MAB004) for 48 hours. For neutralization of hepcidin, spheroids were treated during time of plating with 1 or 3μg/mL of anti-Hepcidin-25 (Amgen, Thousand Oaks, CA (19D12)(71); referred to as αHep#1), anti-Hepcidin-25 (Abcam, Cambridge, MA, USA cat# ab30760; referred to as αHep#2); or anti-IgG (R&D systems, cat#MAB004) for 48 hours. For neutralization of IL-6 in TAF conditioned media, TAF conditioned media was collected as described above and pre-treated with 1 or 5 μg/mL anti-IL-6 or isotope-matched anti-IgG neutralizing antibodies (R&D Systems, cat#MAB2061-100, MAB004) for one hour before addition of CM to TECs during spheroid plating. Human recombinant IL-6 (R&D Systems) was used at 2 and 200 ng/mL. Human recombinant GDF-15 (R&D Systems) was used a 0.1, 0.5, 1, 5, 10, 100 and 200 ng/mL.

Real-time qPCR

RNA was isolated and purified from cells using High Pure RNA Isolation Kit (Roche Diagnostics) following the manufacturer's instructions. Oligo(dT) primer was used in cDNA synthesis. Briefly, 200–400 ng of RNA was reverse transcribed in a total volume of 50 μl with a reverse transcription reagents kit (Applied Biosystems, Foster City, CA, USA). For each comparison, the same amount of RNA was used for reverse transcription. To make a standard curve, serial dilutions of RNA from one sample were added to the RT reaction. Aliquots (2 μl) of cDNA were added to a 18 μl reaction mixture containing 10 μl of 2× SYBR® Green PCR Master Mix (Bio-Rad, Hercules, CA, USA) and 400 nm primers. Three

replicates were run for each sample. See Supplementary Table 3 for primer sequences. Absence of DNA contamination was confirmed by performing PCR from cDNA without reverse transcriptase.

Western Blots

Samples were lysed in 1X RIPA buffer in the presence of protease and phosphatase inhibitors (Roche Diagnostics, Basel, Switzerland) and proteins were separated by SDS-PAGE. Western blots were probed with antibodies to phospho-SMAD-1-5-8 (Cell Signaling Technology, Inc., Danvers, MA, USA; cat#9511), total SMAD-1 (Cell signaling Technology; cat#9743), Phospho-SMAD2-3 (Cell signaling Technology; cat#8828), total-SMAD2/3 (Cell signaling Technology; cat#3102), Phospho-STAT3 (Cell signaling Technology; cat#9131), Total STAT3 (Cell signaling Technology; cat#4904), hepcidin (Fitzgerald Industries International, Acton, MA, USA; cat#70R-6236), Ferroportin (Novus Biologicals, Littleton, CO, USA; cat#NBP1-21502) Ferritin H (72), Ferritin L (Abcam; cat# ab69090), E-Cadherin (Cell signaling Technology; cat# 3195), N Cadherin (Cell signaling Technology; cat# 13116), Vimentin (Cell signaling Technology; cat#5741), Cyclophilin B (Abcam; cat# ab16045) or β-actin (Sigma; cat#A3854). Western blots were quantified with Image J normalized to loading control (β-actin or Cyclophilin B). For western blots in main figures with MCF-7 and MCF-10A cells, three independent experiments were performed. Representative images are displayed with the quantified average of three experiments, including the standard deviation. For western blots utilizing primary patient cells, two independent experiments were performed. Representative images are displayed with the average quantification of two independent experiments. All main figure western blots can be found in their original, uncut versions in the supplemental materials.

Immunofluorescence

Primary patient spheroids were embedded in OCT and sectioned to generate serial cuts that were numbered sequentially from 1–10. When comparing spheroids derived from different cells, section numbers were matched. Sections were fixed with 4% formaldehyde for 15 minutes and blocked with 5% BSA at 4°C overnight. Anti-human ferroportin (Amgen (38C8)) and anti-rabbit Hepcidin (Fitzgerald Industries International; cat#70R-6236) were applied for one hour followed 1:800 dilutions of rhodamine-green conjugated goat anti-human secondary antibody (Jackson ImmunoResearch, West Grove, PA, USA) for ferroportin and Alexa-fluor 555 conjugated goat anti-rabbit IgG secondary antibody (Invitrogen, Carlsbad, CA, USA) for hepcidin. Slides were mounted with ProLong Gold anti-fade reagent (Invitrogen). Images were acquired using a fluorescent inverted microscope (Zeiss Axio Vert.A1; Carl Zeiss Microscopy).

Immunohistochemistry

Primary patient spheroids were embedded in OCT, sectioned and stored in −80° until IHC procedure. Breast tissue microarray slides were obtained from US Biomax, Inc., (Rockville, MD, USA; cat# BR1503e). For both specimen types, antigen retrieval was performed using 0.05% citraconic anhydride (Acros Organics, Geel, Belgium) at pH 7.4 prior to immunostaining. For primary patient spheroids, slides were stained with Hematoxylin and eosin or pan-cytokeratin (AE 1/3) (Cell Signaling Technology) with hematoxylin

counterstain. Images were acquired using a Zeiss Axio Vert.A1 microscope with color Axio Vert.A1 camera (Carl Zeiss Microscopy). For breast tissue microarrays, slides were stained with a rabbit anti-GDF-15 antibody (Sigma-Aldrich; cat# HPA011191) or rabbit anti-Hepcidin antibody (Fitzgerald Industries International, cat#70R-6236). An isotype matched rabbit anti-IgG (Thermo Fisher Scientific; cat#02-6102) was used for negative control and anti-pan keratin (Cell Signaling Technologies; cat#4545) was used to distinguish epithelial from stromal cells. Slides were counterstained with hematoxylin (Poly Scientific R&D Corp., Bay Shore, NY, USA). Images were acquired using a Zeiss Axio Scan Z1 (Carl Zeiss Microscopy) To quantify Hepcidin and GDF-15 expression, stained microarray images were analyzed with Fiji software using reciprocal intensity as previously described (73). Briefly, diaminobenzidine (DAB) signal was isolated from images by color deconvolution. Regions of interest were drawn around epithelial tissue throughout the entire tissue core. Mean DAB intensity/area was then measured in the regions of interest (breast epithelia). Reciprocal intensity (expressed in arbitrary units) was derived by subtracting the maximum intensity value from measured mean DAB intensity/area values. Two cores per patient were used (n=56) and one value was established per patient by normalization with respect to total epithelial cell area. Patients with one or both tissue cores that were negative for anti-pan keratin staining were excluded from quantification analysis. For correlation of staining intensities between Hepcidin and GDF-15, a regression analysis was performed for all included patient samples (n=56).

siRNA Knock-down

All reagents were obtained from GE Dharmacon (Lafayette, CO, USA). ON-TARGETplus human SMARTpools were used for siBMP4 (652; cat#: L-011221-00), siBMP6 (654; cat#; L-021475-00), siBMP7 (655; cat#: L-011592-00), siSTAT3(6774; cat #: L-003544-00), siGDF-15 (9518; cat#: L-019875-00) (referred to as KD#1) and siNTC (cat#: D-001810-10-05) were used for knockdown experiments. ON-TARGETplus individual siRNA human siGDF-15 was used for GDF-15 KD #2 (cat:J-019875-05). siGENOME Control siRNA was used for GAPDH (cat#: D-001140-01-05). Transfections were performed according to the manufacturer's recommendations using Dharmafect #1 (cat: T-2001) transfection reagent. For monolayer cells, knock-down was performed for 24, 48 or 72 hours before harvesting. For spheroids, knock-down was performed in monolayer culture for 24 hours before trypsinization of cells and subsequent spheroid plating. Spheroids were harvested after 3 days, 4 days after initial siRNA transfection. For GDF-15 rescue experiments, recombinant GDF-15 (R&D systems) was added at time of spheroid plating (24 hours after GDF-15 KD). Spheroids were harvested after 3 days (4 days after initial siRNA transfection). KD efficiencies were confirmed at time of harvest by RT-qPCR and/or by ELISA methods described.

ELISA analysis for secreted GDF-15, BMP-6 and IL-6

GDF-15 and IL-6 were measured in conditioned growth media using a GDF-15 or IL-6 Human ELISA kit from R&D systems and following manufacturers' protocol. For siRNA knock-down efficiency, GDF-15 was measured in serum free growth media. BMP-6 was measured in conditioned normal growth media using a Human BMP-6 ELISA kit from Thermo Fisher Scientific and following manufacturers' protocol.

Microarray analysis

MCF-7 cells (monolayer and 3 different 3D culture techniques; pHEMA, mCELL and ULA explained above) were harvested at the day 3 time point and used as samples for microarray analysis. RNA was collected and purified from cell culture lysate using High Pure RNA Isolation Kit (Roche Diagnostics). High quality RNA was submitted to the Yale Center for Genome Analysis (West Haven, CT) for Affymetrix GeneChip analysis of gene expression. Three biological replicates from each condition were hybridized onto the Affymetrix Human Transcriptome Array 2.0 (HTA-2.0) (Thermo Fisher Scientific). Raw CEL files were checked for quality and RMA normalized using Affymetrix Expression Console Software (version 1.4.1.46). Three separate differential expression (DE) analyses were performed for each of the three spheroid culture techniques against monolayer culture using Affymetrix Transcriptome Analysis Software (version 3.0.0.466) with Probeset Annotations release 36 based on UCSC hg19. Significant DE genes were identified based on transcript cluster IDs (probesets) with criteria of ANOVA p value of <0.05 and a fold change greater or less than 2. For compilation of top 10 up-regulated genes, transcript cluster IDs were checked for uniqueness with respect to gene annotation. Additionally, transcript cluster IDs without a corresponding gene symbol or containing _hap (haplotype chromosomes) were discarded. Microarray data associated with this publication can be accessed at the NCBI Gene Expression Omnibus (https://www.ncbi.nlm.nih.gov/geo/) with accession number GSE109733.

GAGE analysis

The transcript cluster ID with the highest average expression per gene in each dataset was selected to represent the expression of that gene. Significantly perturbed KEGG (Kyoto Encyclopedia of Genes and Genomes, [1]) pathways within each dataset were found using the Gene Set Analysis method Generally Applicable Gene-set Enrichment (GAGE), since it is optimized for use with both small and large datasets [2], using the bidirectional option (same.dir=F) and unpaired sample setting (compare="unpaired").

TCGA analysis

Lowess-normalized gene-level mRNA expression data from Agilent custom whole genome microarrays (TCGA, BRCA, 2012; PMID: 23000897) of primary breast cancer samples were uploaded on 10-24-16 from the Broad Firehose (https://gdac.broadinstitute.org/), along with clinical and biospeciman supporting data (49). For each sample, GDF-15 and HAMP expression was extracted. Samples were classified as 'cancer' if the 'Sample' identifier of the sample barcode was 01a or 01b and samples were classified as 'normal' if the 'sample' identifier of the sample barcode was 11a or 11b, based on identification between the sample identifier and the sample type in the biospecimen data. All statistical analyses were performed in Prism 6. For comparison of GDF-15 and HAMP expression, respectively, between the normal and cancer samples, and of GDF-15 expression between low and high HAMP cancer samples, a two-tailed unpaired Student's t test was used.

Statistical analysis

All experiments were performed at least three times using a minimum of three replicates/condition in each experiment. Results of representative experiments are shown in the figures. Statistical analyses were performed using Excel or Prism 6 (Graphpad software) and are reported as the mean ± standard deviation. Error bars represent standard deviation. Unless otherwise noted, significant differences between control and treatment groups were determined using two-tailed unpaired Student's t tests.

Supplementary Material

Refer to Web version on PubMed Central for supplementary material.

Acknowledgments

This work was supported in part by NCI R01CA188025 (SVT), NCI R01CA171101 (FMT) and NCI F32CA214030 (AK). We thank Li Chen and Drs. Nathaniel Dyment and David Rowe for assistance in image acquisition, Tara L Arvedson (Amgen, Thousand Oaks, CA) for a generous gift of anti-ferroportin antibody and Xiaohong Wang for her assistance in histological sectioning.

References

1Tonik SE, Shindelman JE, Sussman HH. Transferrin receptor is inversely correlated with estrogen receptor in breast cancer. Breast cancer research and treatment. 1986; 7(2):71–6. [PubMed: 3013349]

2Daniels TR, Bernabeu E, Rodriguez JA, Patel S, Kozman M, Chiappetta DA, et al. The transferrin receptor and the targeted delivery of therapeutic agents against cancer. Biochim Biophys Acta. 2012; 1820(3):291–317. [PubMed: 21851850]

3Wrba F, Ritzinger E, Reiner A, Holzner JH. Transferrin receptor (TrfR) expression in breast carcinoma and its possible relationship to prognosis. An immunohistochemical study. Virchows Archiv A, Pathological anatomy and histopathology. 1986; 410(1):69–73. [PubMed: 3024390]

4Wang W, Deng Z, Hatcher H, Miller LD, Di X, Tesfay L, et al. IRP2 regulates breast tumor growth. Cancer research. 2014; 74(2):497–507. [PubMed: 24285726]

5Pinnix ZK, Miller LD, Wang W, D'Agostino R Jr, Kute T, Willingham MC, et al. Ferroportin and iron regulation in breast cancer progression and prognosis. Science translational medicine. 2010; 2(43): 43ra56.

6Zhang S, Chen Y, Guo W, Yuan L, Zhang D, Xu Y, et al. Disordered hepcidin-ferroportin signaling promotes breast cancer growth. Cell Signal. 2014; 26(11):2539–50. [PubMed: 25093806]

7Nemeth E, Tuttle MS, Powelson J, Vaughn MB, Donovan A, Ward DM, et al. Hepcidin regulates cellular iron efflux by binding to ferroportin and inducing its internalization. Science. 2004; 306(5704):2090–3. [PubMed: 15514116]

8Abboud S, Haile DJ. A novel mammalian iron-regulated protein involved in intracellular iron metabolism. The Journal of biological chemistry. 2000; 275(26):19906–12. [PubMed: 10747949]

9Donovan A, Brownlie A, Zhou Y, Shepard J, Pratt SJ, Moynihan J, et al. Positional cloning of zebrafish ferroportin1 identifies a conserved vertebrate iron exporter. Nature. 2000; 403(6771):776–81. [PubMed: 10693807]

10McKie AT, Marciani P, Rolfs A, Brennan K, Wehr K, Barrow D, et al. A novel duodenal iron-regulated transporter, IREG1, implicated in the basolateral transfer of iron to the circulation. Mol Cell. 2000; 5(2):299–309. [PubMed: 10882071]

11Babitt JL, Huang FW, Xia Y, Sidis Y, Andrews NC, Lin HY. Modulation of bone morphogenetic protein signaling in vivo regulates systemic iron balance. J Clin Invest. 2007; 117(7):1933–9. [PubMed: 17607365]

12Andriopoulos B Jr, Corradini E, Xia Y, Faasse SA, Chen S, Grgurevic L, et al. BMP6 is a key endogenous regulator of hepcidin expression and iron metabolism. Nat Genet. 2009; 41(4):482–7. [PubMed: 19252486]

13Lee P, Peng H, Gelbart T, Wang L, Beutler E. Regulation of hepcidin transcription by interleukin-1 and interleukin-6. Proc Natl Acad Sci U S A. 2005; 102(6):1906–10. [PubMed: 15684062]

14Lee GY, Kenny PA, Lee EH, Bissell MJ. Three-dimensional culture models of normal and malignant breast epithelial cells. Nat Methods. 2007; 4(4):359–65. [PubMed: 17396127]

15Kim JB, Stein R, O'Hare MJ. Three-dimensional in vitro tissue culture models of breast cancer-- a review. Breast Cancer Res Treat. 2004; 85(3):281–91. [PubMed: 15111767]

16Bissell MJ, Hall HG, Parry G. How does the extracellular matrix direct gene expression? Journal of theoretical biology. 1982; 99(1):31–68. [PubMed: 6892044]

17Debnath J, Brugge JS. Modelling glandular epithelial cancers in three-dimensional cultures. Nat Rev Cancer. 2005; 5(9):675–88. [PubMed: 16148884]

18Weigelt B, Bissell MJ. Unraveling the microenvironmental influences on the normal mammary gland and breast cancer. Semin Cancer Biol. 2008; 18(5):311–21. [PubMed: 18455428]

19Liu X, Ory V, Chapman S, Yuan H, Albanese C, Kallakury B, et al. ROCK inhibitor and feeder cells induce the conditional reprogramming of epithelial cells. The American journal of pathology. 2012; 180(2):599–607. [PubMed: 22189618]

20Liu X, Krawczyk E, Suprynowicz FA, Palechor-Ceron N, Yuan H, Dakic A, et al. Conditional reprogramming and long-term expansion of normal and tumor cells from human biospecimens. Nature protocols. 2017; 12(2):439–51. [PubMed: 28125105]

21Soule HD, Vazguez J, Long A, Albert S, Brennan M. A human cell line from a pleural effusion derived from a breast carcinoma. J Natl Cancer Inst. 1973; 51(5):1409–16. [PubMed: 4357757]

22Wrighting DM, Andrews NC. Interleukin-6 induces hepcidin expression through STAT3. Blood. 2006; 108(9):3204–9. [PubMed: 16835372]

23Arman A, Auron PE. Interleukin 1 (IL-1) induces the activation of Stat3. Adv Exp Med Biol. 2003; 534:297–307. [PubMed: 12903728]

24Caldenhoven E, van Dijk T, Raaijmakers JA, Lammers JW, Koenderman L, De Groot RP. Activation of the STAT3/acute phase response factor transcription factor by interleukin-5. J Biol Chem. 1995; 270(43):25778–84. [PubMed: 7592760]

25Yang CH, Murti A, Pfeffer LM. STAT3 complements defects in an interferon-resistant cell line: evidence for an essential role for STAT3 in interferon signaling and biological activities. Proc Natl Acad Sci U S A. 1998; 95(10):5568–72. [PubMed: 9576923]

26Garcia R, Bowman TL, Niu G, Yu H, Minton S, Muro-Cacho CA, et al. Constitutive activation of Stat3 by the Src and JAK tyrosine kinases participates in growth regulation of human breast carcinoma cells. Oncogene. 2001; 20(20):2499–513. [PubMed: 11420660]

27Schafer ZT, Grassian AR, Song L, Jiang Z, Gerhart-Hines Z, Irie HY, et al. Antioxidant and oncogene rescue of metabolic defects caused by loss of matrix attachment. Nature. 2009; 461(7260):109–13. [PubMed: 19693011]

28Coloff JL, Murphy JP, Braun CR, Harris IS, Shelton LM, Kami K, et al. Differential Glutamate Metabolism in Proliferating and Quiescent Mammary Epithelial Cells. Cell Metab. 2016; 23(5): 867–80. [PubMed: 27133130]

29Saias L, Gomes A, Cazales M, Ducommun B, Lobjois V. Cell-Cell Adhesion and Cytoskeleton Tension Oppose Each Other in Regulating Tumor Cell Aggregation. Cancer Res. 2015; 75(12): 2426–33. [PubMed: 25855380]

30Perou CM, Jeffrey SS, van de Rijn M, Rees CA, Eisen MB, Ross DT, et al. Distinctive gene expression patterns in human mammary epithelial cells and breast cancers. Proc Natl Acad Sci U S A. 1999; 96(16):9212–7. [PubMed: 10430922]

31Nieman MT, Prudoff RS, Johnson KR, Wheelock MJ. N-cadherin promotes motility in human breast cancer cells regardless of their E-cadherin expression. J Cell Biol. 1999; 147(3):631–44. [PubMed: 10545506]

32Torti FM, Torti SV. Regulation of ferritin genes and protein. Blood. 2002; 99(10):3505–16. [PubMed: 11986201]

33Hentze MW, Caughman SW, Rouault TA, Barriocanal JG, Dancis A, Harford JB, et al. Identification of the iron-responsive element for the translational regulation of human ferritin mRNA. Science. 1987; 238(4833):1570–3. [PubMed: 3685996]

34Arosio P, Levi S. Cytosolic and mitochondrial ferritins in the regulation of cellular iron homeostasis and oxidative damage. Biochim Biophys Acta. 2010; 1800(8):783–92. [PubMed: 20176086]

35Theil EC, Tosha T, Behera RK. Solving Biology's Iron Chemistry Problem with Ferritin Protein Nanocages. Acc Chem Res. 2016; 49(5):784–91. [PubMed: 27136423]

36Longati P, Jia X, Eimer J, Wagman A, Witt MR, Rehnmark S, et al. 3D pancreatic carcinoma spheroids induce a matrix-rich, chemoresistant phenotype offering a better model for drug testing. BMC Cancer. 2013; 13:95. [PubMed: 23446043]

37Yu M, Lin G, Arshadi N, Kalatskaya I, Xue B, Haider S, et al. Expression profiling during mammary epithelial cell three-dimensional morphogenesis identifies PTPRO as a novel regulator of morphogenesis and ErbB2-mediated transformation. Molecular and cellular biology. 2012; 32(19):3913–24. [PubMed: 22851698]

38Francia G, Man S, Teicher B, Grasso L, Kerbel RS. Gene expression analysis of tumor spheroids reveals a role for suppressed DNA mismatch repair in multicellular resistance to alkylating agents. Molecular and cellular biology. 2004; 24(15):6837–49. [PubMed: 15254249]

39Riedl A, Schlederer M, Pudelko K, Stadler M, Walter S, Unterleuthner D, et al. Comparison of cancer cells in 2D vs 3D culture reveals differences in AKT-mTOR-S6K signaling and drug responses. J Cell Sci. 2017; 130(1):203–18. [PubMed: 27663511]

40Bootcov MR, Bauskin AR, Valenzuela SM, Moore AG, Bansal M, He XY, et al. MIC-1, a novel macrophage inhibitory cytokine, is a divergent member of the TGF-beta superfamily. Proc Natl Acad Sci U S A. 1997; 94(21):11514–9. [PubMed: 9326641]

41Welsh JB, Sapinoso LM, Kern SG, Brown DA, Liu T, Bauskin AR, et al. Large-scale delineation of secreted protein biomarkers overexpressed in cancer tissue and serum. Proc Natl Acad Sci U S A. 2003; 100(6):3410–5. [PubMed: 12624183]

42Yalcin MM, Altinova AE, Akturk M, Gulbahar O, Arslan E, Ors Sendogan D, et al. GDF-15 and Hepcidin Levels in Nonanemic Patients with Impaired Glucose Tolerance. J Diabetes Res. 2016; 2016:1240843. [PubMed: 27642607]

43Yilmaz H, Cakmak M, Darcin T, Inan O, Bilgic MA, Bavbek N, et al. Can Serum Gdf-15 be Associated with Functional Iron Deficiency in Hemodialysis Patients? Indian J Hematol Blood Transfus. 2016; 32(2):221–7. [PubMed: 27065587]

44Tanno T, Bhanu NV, Oneal PA, Goh SH, Staker P, Lee YT, et al. High levels of GDF15 in thalassemia suppress expression of the iron regulatory protein hepcidin. Nat Med. 2007; 13(9): 1096–101. [PubMed: 17721544]

45Winand FJ, et al. GDF15 and Hepcidin as Prognostic Factors in Patients with Prostate Cancer. Journal of Molecular Biomarkers & Diagnosis. 2014; 05(06)

46Li C, Wang J, Kong J, Tang J, Wu Y, Xu E, et al. GDF15 promotes EMT and metastasis in colorectal cancer. Oncotarget. 2016; 7(1):860–72. [PubMed: 26497212]

47Li YL, Chang JT, Lee LY, Fan KH, Lu YC, Li YC, et al. GDF15 contributes to radioresistance and cancer stemness of head and neck cancer by regulating cellular reactive oxygen species via a SMAD-associated signaling pathway. Oncotarget. 2017; 8(1):1508–28. [PubMed: 27903972]

48Wrana JL. Regulation of Smad activity. Cell. 2000; 100(2):189–92. [PubMed: 10660041]

49Comprehensive molecular portraits of human breast tumours. Nature. 2012; 490(7418):61–70. [PubMed: 23000897]

50Hanahan D, Coussens LM. Accessories to the crime: functions of cells recruited to the tumor microenvironment. Cancer Cell. 2012; 21(3):309–22. [PubMed: 22439926]

51Kenny PA, Lee GY, Myers CA, Neve RM, Semeiks JR, Spellman PT, et al. The morphologies of breast cancer cell lines in three-dimensional assays correlate with their profiles of gene expression. Mol Oncol. 2007; 1(1):84–96. [PubMed: 18516279]

52Martin KJ, Patrick DR, Bissell MJ, Fournier MV. Prognostic breast cancer signature identified from 3D culture model accurately predicts clinical outcome across independent datasets. PLoS One. 2008; 3(8):e2994. [PubMed: 18714348]

53Horning JL, Sahoo SK, Vijayaraghavalu S, Dimitrijevic S, Vasir JK, Jain TK, et al. 3-D tumor model for in vitro evaluation of anticancer drugs. Mol Pharm. 2008; 5(5):849–62. [PubMed: 18680382]

54Nath S, Devi GR. Three-dimensional culture systems in cancer research: Focus on tumor spheroid model. Pharmacol Ther. 2016; 163:94–108. [PubMed: 27063403]

55Fairlie WD, Moore AG, Bauskin AR, Russell PK, Zhang HP, Breit SN. MIC-1 is a novel TGF-beta superfamily cytokine associated with macrophage activation. J Leukoc Biol. 1999; 65(1):2–5. [PubMed: 9886240]

56Schober A, Bottner M, Strelau J, Kinscherf R, Bonaterra GA, Barth M, et al. Expression of growth differentiation factor-15/macrophage inhibitory cytokine-1 (GDF-15/MIC-1) in the perinatal, adult, and injured rat brain. J Comp Neurol. 2001; 439(1):32–45. [PubMed: 11579380]

57Franca Julia W, Martin B, Inka G, Lothar H, Axel S, Maria E, et al. GDF15 and Hepcidin as Prognostic Factors in Patients with Prostate Cancer. 2014; 5(6)

58Park YJ, Lee H, Lee JH. Macrophage inhibitory cytokine-1 transactivates ErbB family receptors via the activation of Src in SK-BR-3 human breast cancer cells. BMB Rep. 2010; 43(2):91–6. [PubMed: 20193126]

59Sasahara A, Tominaga K, Nishimura T, Yano M, Kiyokawa E, Noguchi M, et al. An autocrine/paracrine circuit of growth differentiation factor (GDF) 15 has a role for maintenance of breast cancer stem-like cells. Oncotarget. 2017; 8(15):24869–81. [PubMed: 28206960]

60Meynard D, Kautz L, Darnaud V, Canonne-Hergaux F, Coppin H, Roth MP. Lack of the bone morphogenetic protein BMP6 induces massive iron overload. Nat Genet. 2009; 41(4):478–81. [PubMed: 19252488]

61Pickl M, Ries CH. Comparison of 3D and 2D tumor models reveals enhanced HER2 activation in 3D associated with an increased response to trastuzumab. Oncogene. 2009; 28(3):461–8. [PubMed: 18978815]

62Aboussekhra A. Role of cancer-associated fibroblasts in breast cancer development and prognosis. Int J Dev Biol. 2011; 55(7–9):841–9. [PubMed: 22161840]

63Allinen M, Beroukhim R, Cai L, Brennan C, Lahti-Domenici J, Huang H, et al. Molecular characterization of the tumor microenvironment in breast cancer. Cancer Cell. 2004; 6(1):17–32. [PubMed: 15261139]

64Whiteside TL. The tumor microenvironment and its role in promoting tumor growth. Oncogene. 2008; 27(45):5904–12. [PubMed: 18836471]

65Marques O, Porto G, Rema A, Faria F, Cruz Paula A, Gomez-Lazaro M, et al. Local iron homeostasis in the breast ductal carcinoma microenvironment. BMC Cancer. 2016; 16:187. [PubMed: 26944411]

66Bruzzese F, Hagglof C, Leone A, Sjoberg E, Roca MS, Kiflemariam S, et al. Local and systemic protumorigenic effects of cancer-associated fibroblast-derived GDF15. Cancer Res. 2014; 74(13): 3408–17. [PubMed: 24780757]

67Tesfay L, Clausen KA, Kim JW, Hegde P, Wang X, Miller LD, et al. Hepcidin regulation in prostate and its disruption in prostate cancer. Cancer Res. 2015; 75(11):2254–63. [PubMed: 25858146]

68Howlader N, Altekruse SF, Li CI, Chen VW, Clarke CA, Ries LA, et al. US incidence of breast cancer subtypes defined by joint hormone receptor and HER2 status. J Natl Cancer Inst. 2014; 106(5)

69Perou CM, Sorlie T, Eisen MB, van de Rijn M, Jeffrey SS, Rees CA, et al. Molecular portraits of human breast tumours. Nature. 2000; 406(6797):747–52. [PubMed: 10963602]

70Sorlie T, Perou CM, Tibshirani R, Aas T, Geisler S, Johnsen H, et al. Gene expression patterns of breast carcinomas distinguish tumor subclasses with clinical implications. Proc Natl Acad Sci U S A. 2001; 98(19):10869–74. [PubMed: 11553815]

71Cooke KS, Hinkle B, Salimi-Moosavi H, Foltz I, King C, Rathanaswami P, et al. A fully human anti-hepcidin antibody modulates iron metabolism in both mice and nonhuman primates. Blood. 2013; 122(17):3054–61. [PubMed: 23945155]

72Wilkinson Jt, Pietsch EC, , Torti SV, , Torti FM. Ferritin regulation by oxidants and chemopreventive xenobiotics. Advances in enzyme regulation. 2003; 43:135–51. [PubMed: 12791388]

73Nguyen D. Quantifying chromogen intensity in immunohistochemistry via reciprocal intensity. 2013

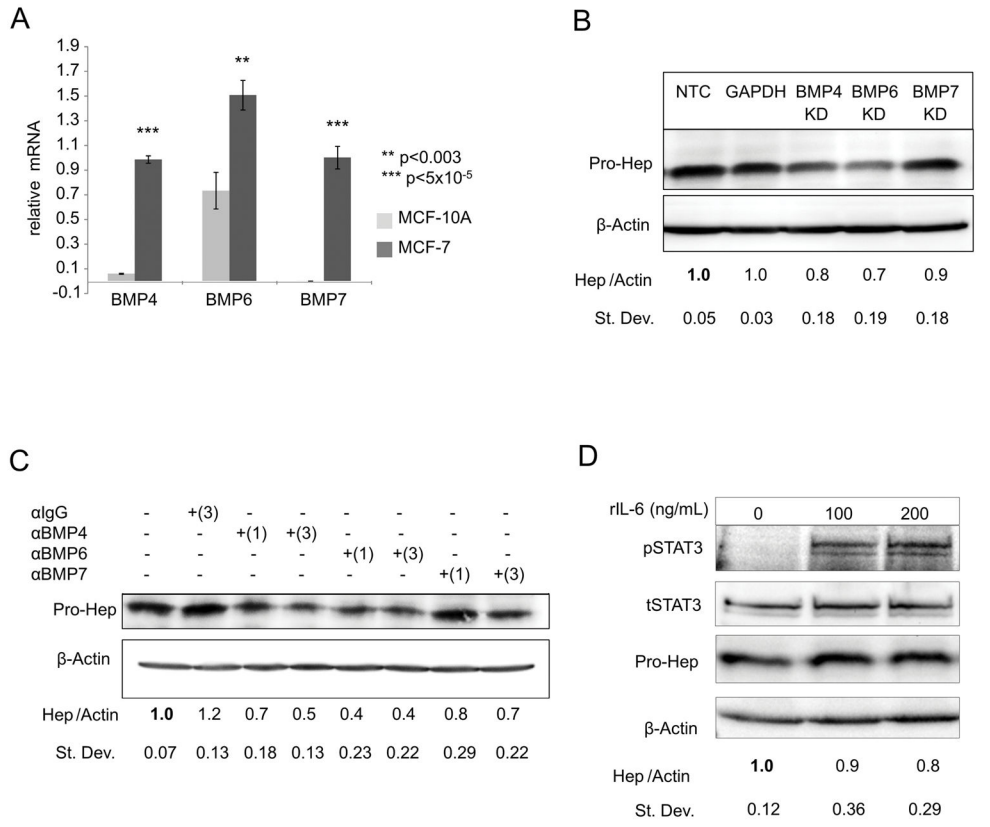

Figure 1. BMPs regulate hepcidin expression in MCF-7 breast cancer cells

(A) RT-qPCR of BMP4, BMP6 or BMP7 mRNA (normalized to β-actin) in MCF-7 and MCF-10A monolayer cells. (B) Western blot analysis of pro-hepcidin and β-actin following siRNA knock-down of non-target control (NTC), BMP4, BMP6, and BMP7 for 48 hours in MCF-7 cells. For quantification, samples were compared to NTC. GAPDH siRNA was used as an additional control. (C) Western blot analysis of pro-hepcidin and β-actin after the addition of 1 and 3 μg/mL neutralizing antibodies against BMP4, BMP6, BMP7 or IgG (3μg/ml) isotope control for 48 hrs in MCF-7 cells. For quantification, samples were compared to untreated sample. (D) Western blot analysis of phosporylated-STAT3 (pSTAT3), total STAT3 (tSTAT3), pro-hepcidin, and β-actin following the addition of recombinant IL-6 for 24 hours in MCF-7 cells.

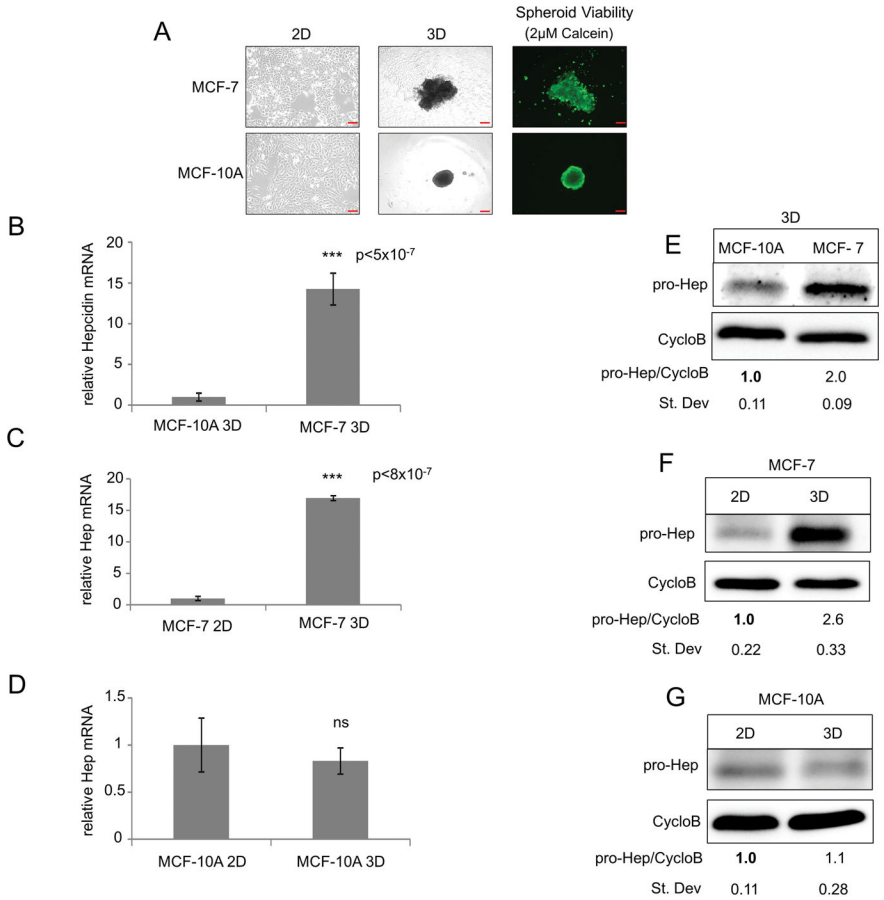

Figure 2. Hepcidin is increased in MCF-7 breast cancer spheroids compared to non-tumor spheroids and is induced from 2D to 3D culture of breast cancer cells

(A) Phase-contrast imaging of MCF-7 and MCF-10A cells grown in 2D and 3D and fluorescent imaging of spheroids stained with 2μM calcein-AM. (B–D) RT-qPCR of hepcidin mRNA (normalized to cyclophilin A) in MCF-7 and MCF-10A cells grown in 2D and 3D. (E–G) Western blot of pro-hepcidin using Cyclophilin B as internal control. Scale bar: 10μm (2D), 200μm (3D)

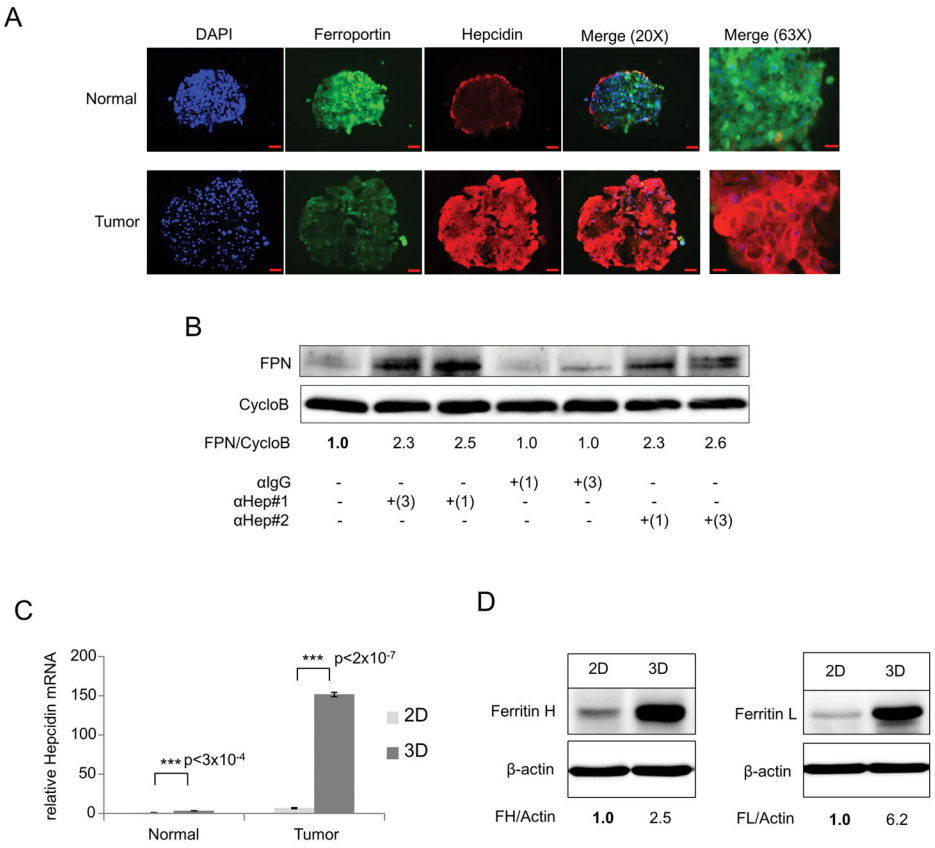

Figure 3. Hepcidin is increased in primary patient breast cancer spheroids, degrades FPN and is associated with an increase in the iron storage protein ferritin

(A) Immunofluorescence staining of FPN (green) Hep (red) and DAPI (blue) in primary breast spheroid sections from patient 107 normal and tumor. The hepcidin antibody used in this experiment is directed at an epitope found in the hepcidin precursor (Fitzgerald Industries International, Acton, MA, USA). (B) Western blot analysis of Ferroportin (FPN) and Cyclophilin B (CycloB) following 48 hours of treatment with 1 or 3 μg/mL neutralizing anti-hepcidin antibody directed at secreted Hepcidin-25 (#1 Amgen, #2 Abcam) or isotope-matched anti-IgG control in patient 107 tumor spheroids. For quantification, samples were compared to untreated sample. (C) RT-qPCR of Hepcidin mRNA (normalized to Cyclophilin A) in patient 107 normal and tumor patient breast cells grown as monolayer or spheroids. (D) Western blot analysis of Ferritin H, Ferritin L and β-actin of patient 107 tumor monolayer and spheroids. Scale bar 50μm (20X); 20μm (63X).

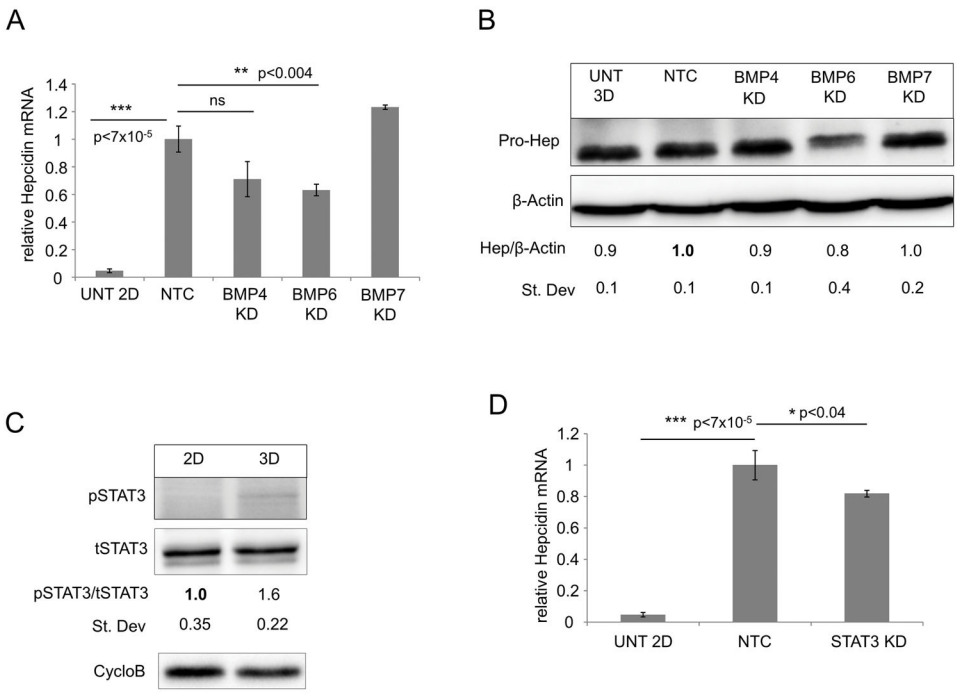

Figure 4. Known regulators of hepcidin have a modest effect on regulation of hepcidin in breast cancer spheroids

(A) RT-qPCR of Hepcidin mRNA (normalized to Cyclophilin A) and (B) western blot analysis of pro-hepcidin and β-actin following siRNA knock-down of non-target control (NTC), BMP4, BMP6, and BMP7 in MCF-7 spheroids. Untreated MCF-7 cells grown in 2D (A) or 3D (B) were used as controls. Statistical analysis and quantification was normalized to non-targeting control siRNA. (C) Western blot analysis of p-STAT3, total STAT-3 and Cyclophilin B in MCF-7 monolayer versus spheroids cultured for 3 days. (D) RT-qPCR of hepcidin mRNA (normalized to Cyclophilin A) following siRNA knock-down of NTC and STAT3 in MCF-7 spheroids. For statistical analysis samples were compared to non-targeting control. Untreated MCF-7 2D was used as a control.

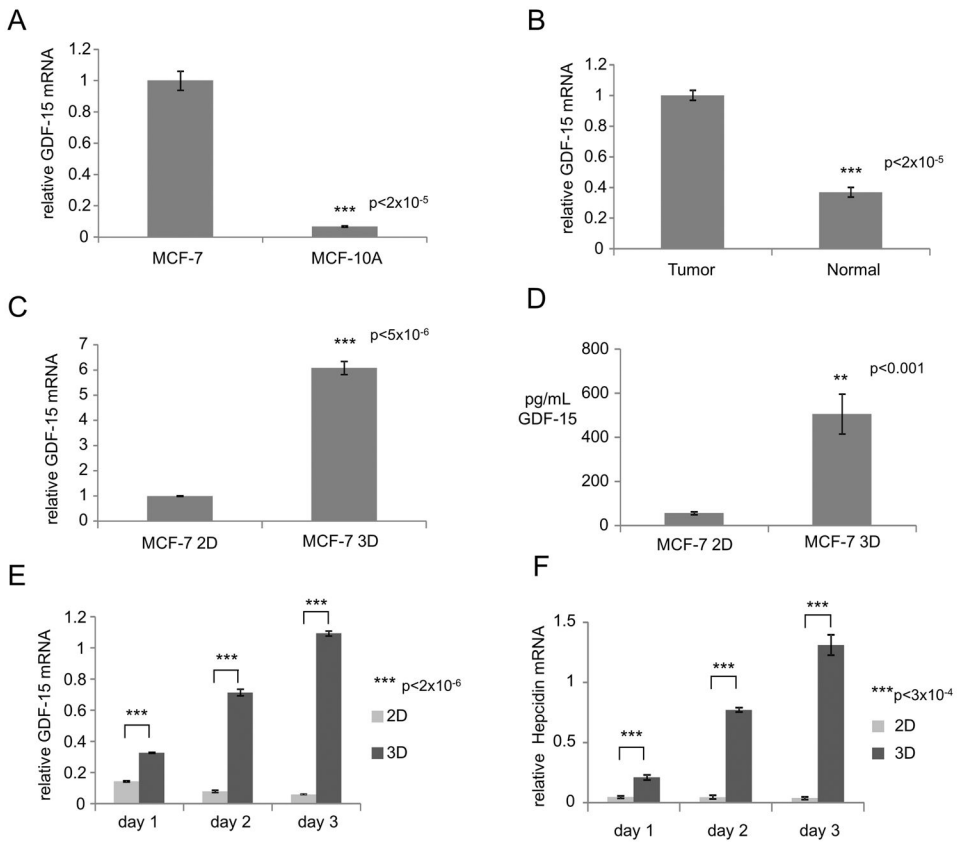

Figure 5. GDF-15 is induced in breast cancer spheroids and correlates with hepcidin expression

(A–C) RT-qPCR of GDF-15 mRNA (normalized to Cyclophilin A) between (A) MCF-7 and MCF-10A spheroids, (B) patient 107 tumor vs. normal adjacent tumor (normal) spheroids and (C) MCF-7 monolayer vs. MCF-7 spheroids. (D) Secreted GDF-15 from conditioned media of MCF-7 monolayer and spheroids normalized to μg protein. (E–F) RT-qPCR of (E) GDF-15 mRNA (normalized to Cyclophilin A) and (F) hepcidin mRNA (normalized to Cyclophilin A) in MCF-7 monolayer (2D) and spheroids (3D) over time.

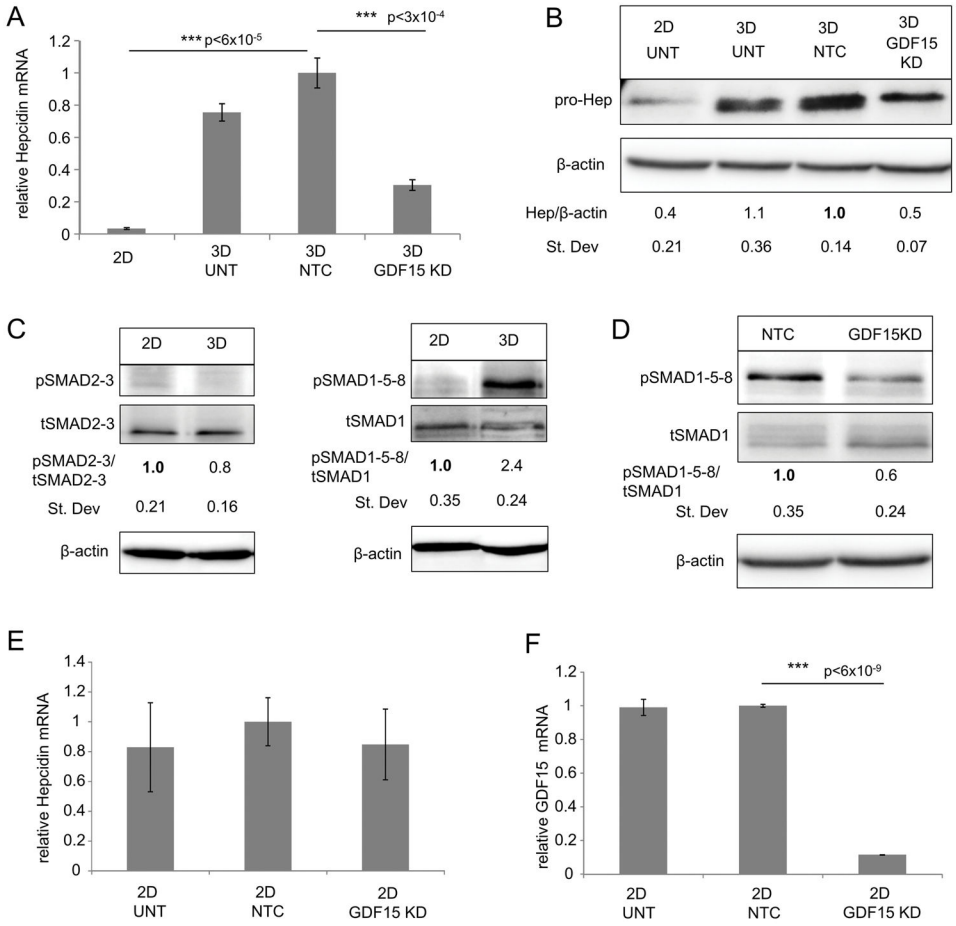

Figure 6. GDF-15 positively regulates hepcidin in breast cancer spheroids via a conserved pSMAD1-5-8 pathway

(A) RT-qPCR of Hepcidin mRNA (normalized to Cyclophilin A) and (B) western blot analysis of pro-hepcidin and β-actin following knock-down using non targeting control (NTC) siRNA and GDF-15 siRNA (KD#1) in MCF-7 spheroids. Untreated MCF-7 cells grown in 2D or 3D were used as controls. For statistical analysis and quantification, samples were compared to non-targeting control. (C) Western blot analysis of phosphorylated SMAD2-3, total SMAD2, phosphorylated SMAD1-5-8, total SMAD-1, and β-actin in MCF-7 monolayers and spheroids. (D) Western blot analysis of pSMAD1-5-8, tSMAD-1 and β-actin following siRNA knock-down of NTC and GDF-15 knock-down #1. (E–F) RT-qPCR of (E) hepcidin mRNA (normalized to Cyclophilin A) and (F) GDF-15 mRNA (normalized to Cyclophiin A) following siRNA knock-down of NTC and GDF-15 knock-down #1 for 3 days in MCF-7 monolayer. For statistical analysis, samples were compared to non-targeting control.

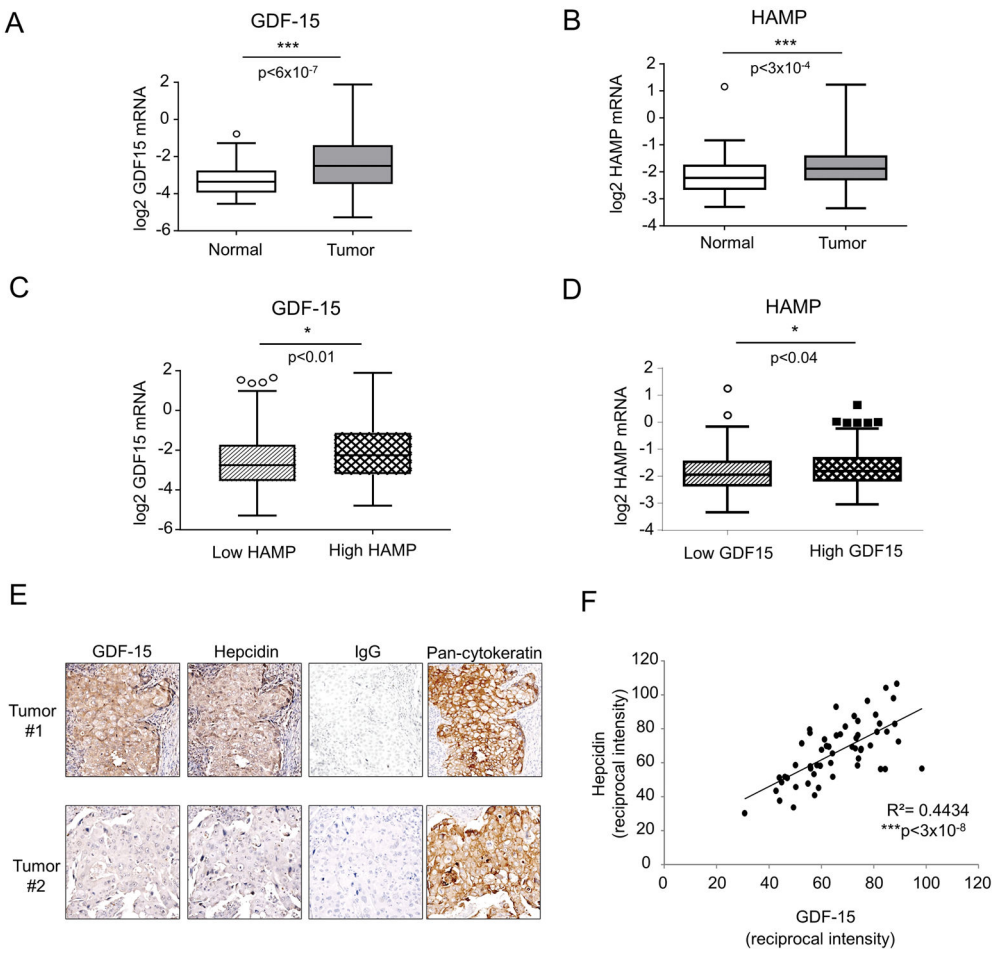

Figure 7. Hepcidin and GDF-15 are increased and their expression is correlated in breast tumors

(A and B) Box plot with Tukey whisker of (A) *GDF15* and (B) *HAMP* mRNA expression (log2 transformed) in normal adjacent tissue (n=61) compared to primary tumor tissue (n=526) in the TCGA breast cancer dataset. (C) *GDF15* transcripts in TCGA samples from breast cancer patients divided by *HAMP* expression (below and above the mean) shown as box and whisker plot. (D) *HAMP* transcripts in TCGA samples from breast cancer patients divided by *GDF15* expression (below and above the mean) shown as box and whisker. (E) Representative images of immunohistochemical staining of tumor tissue from patients with invasive ductal carcinoma (IDC). Proteins stained are Hepcidin, GDF-15, Pan-Cytokeratin and IgG control. (F) Scatter plot displays quantification of staining of epithelial cells from tissues from 56 BRCA patients. A regression analysis was performed to examine correlation of staining intensities (R^2=0.4434 $p<3\times10^{-8}$).

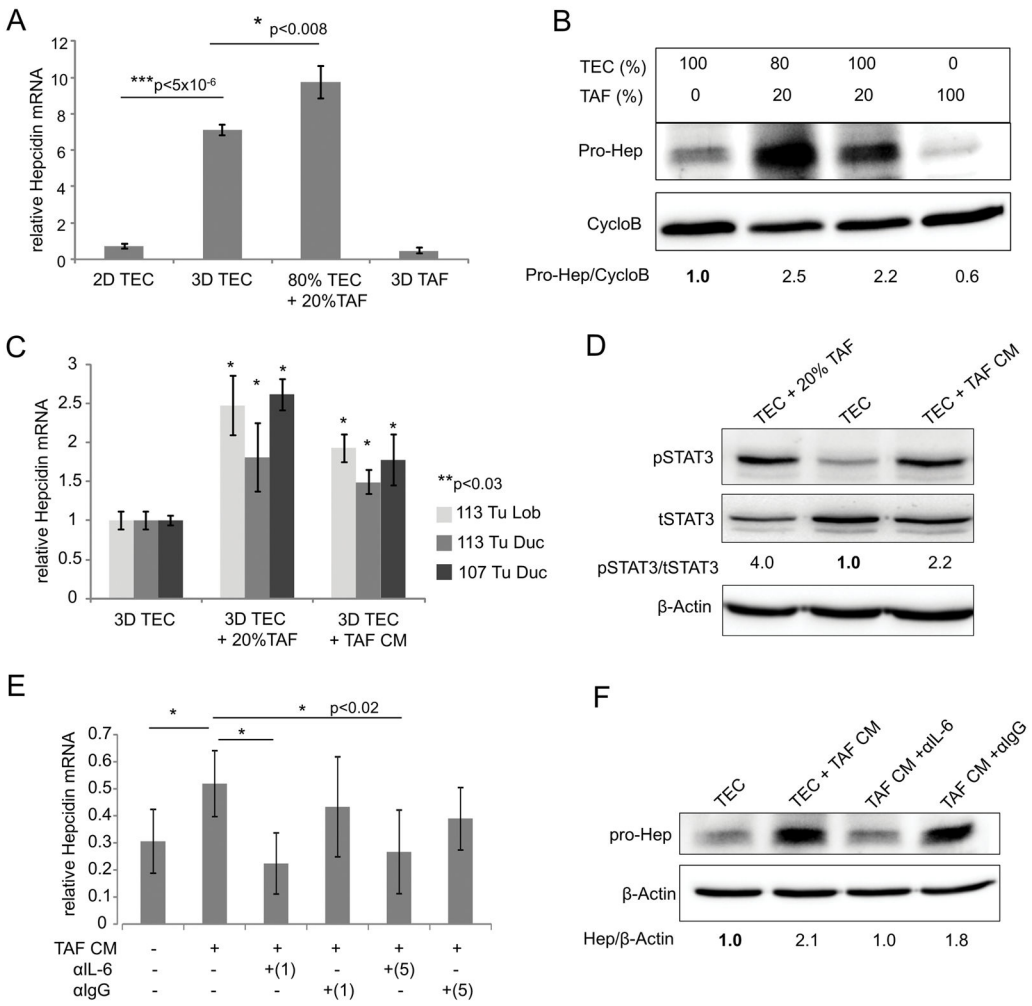

Figure 8. IL-6 secreted by tumor associated fibroblasts (TAFs) induces hepcidin in breast cancer spheroids

(A) RT-qPCR of hepcidin mRNA (normalized to Cyclophilin A) in patient 113 lobular epithelial cell samples. Samples were 100% 2D tumor epithelial cells (2D TEC), 100% tumor epithelial cell spheroids (3D TEC), spheroids composed of a mixture of 80% TEC and 20% irradiated TAFs (isolated from patient 113), (80% TEC +20%TAF) and 100% irradiated TAF spheroids after 3 days of culture. (B) Western blot analysis of pro-hepcidin and Cyclophilin B for different TEC/TAF (%) combinations after 3 days of spheroid culture. (C) RT-qPCR of hepcidin mRNA (normalized to Cyclophilin A) and (D) western blot analysis of phosphorylated and total STAT3 of primary TEC spheroids alone, spheroids composed of a mixture of 80% TECs and 20%TAFs, or TEC spheroids exposed to conditioned media (CM) from TAFs for 4 days. Patient 113 tumor ductal (113 Tu Duc), patient 113 tumor lobular (113 Tu Lob) and patient 107 tumor ductal (107 Tu Duc) were used for (C) and patient 113 tumor lobular for (D). For statistical analysis in (C) samples with 20% TAF or TAF CM were compared to their respective 3D TEC sample. (E) RT-qPCR of hepcidin mRNA (normalized to Cyclophilin A) of patient 113 lobular TEC spheroids after the addition of TAF CM and IL-6 neutralizing antibody (1=1μg/mL and 5=5μg/mL) for 4 days. Neutralizing antibody against IgG (1 and 5 μg/mL) was used as a control. For

statistical analysis, samples were compared to TAF CM sample. (F) Western blot analysis of pro-hepcidin and β-actin of patient 113 lobular TEC spheroids after the addition of TAF CM with or without 1μg/mL neutralizing antibodies against IL-6 or IgG for 4 days. All western blot quantifications (B, D and F) were compared to TEC alone.

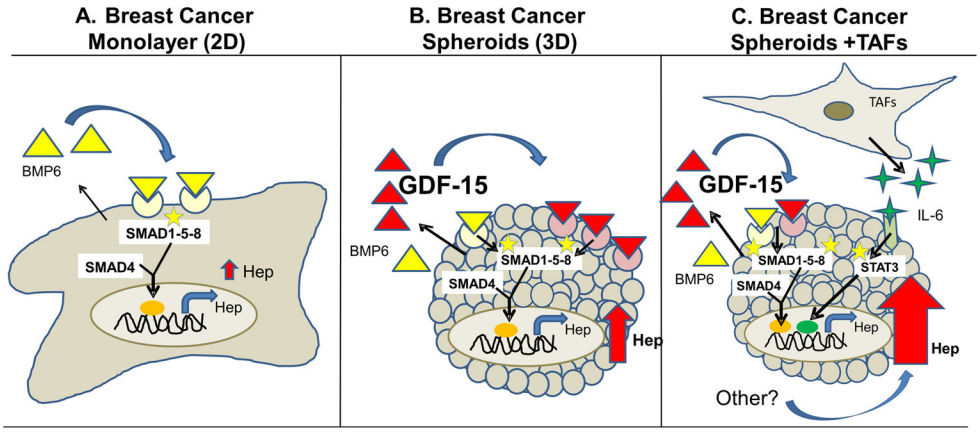

Figure 9. Working model of regulation of hepcidin in breast cancer spheroids

Hepcidin expression is increased in breast cancer cells relative to non-cancer cells. A. In MCF-7 cells grown as 2D monolayers, BMP6 plays a dominant role in the cancer-dependent increase in hepcidin through activation of a SMAD1-5-8 signaling pathway. B. In breast cancer spheroids, spatial control of hepcidin synthesis is exerted by GDF-15, which augments SMAD 1-5- 8 signaling to further increase hepcidin synthesis. C. The microenvironment is an additional source for increased hepcidin in breast cancer cells, in part due to production of IL-6 by tumor-associated fibroblasts (TAFs).

Table 1

Clinical characteristics of primary breast tumor samples.

Patient #	Patient Age	Tumor Type	Tumor Grade (Nottingham)	Tumor Size	ER Status	PR Status	HER2 Status (IHC)	HER2 Status (FISH)	Nodal Status	TNM
107	68	Ductal	I	1.5×1.0×0.5	± (3/8)	− (0/8)	− (1/3)	N/A	0	pT1cN0MX
109	80	Mucinous	I	2.8 × 1.1	+ (8/8)	± (4/8)	− (0/3)	N/A	0	pT2NXMX
113	53	Ductal (Left)	I	8.5×8.0×3.8	+ (5/8)	− (0/8)	− (0/3)	N/A	0	pTisN0MX
		Lobular (Right)	II	5cm	+ (8/8)	+ (8/8)	± (2/3)	− (0/3)	0	pT3N0MX
129	65	Ductal	II	2.1cm	+ (8/8)	+ (7/8)	± (2/3)	− (0/3)	Pos (0.56mm) micro FISH 1.3	pTpN1micpMX

All tumor samples were de-identified at time of obtainment. Clinical pathology was performed and recorded for each patient. (ER) estrogen receptor, (PR) progesterone receptor, (Her2) human epidermal growth factor receptor 2, (TNM) tumor node metastasis, (IHC) Immunohistochemistry, (FISH) Fluorescence in situ hybridization.

Table 2

Top 10 upregulated genes in 3D culture from differential expression analysis between monolayer and three spheroid conditions.

	polyHEMA (pHEMA)					Ultra-low attachment (ULA)					Methylcellulose (mCELL)				
Rank	**Fold Change (linear)**	**ANOVA p-value**	**FDR p-value**	**Gene Symbol**	**Description**	**Fold Change (linear)**	**ANOVA p-value**	**FDR p-value**	**Gene Symbol**	**Description**	**Fold Change (linear)**	**ANOVA p-value**	**FDR p-value**	**Gene Symbol**	**Description**
1	47.93	1.79E-07	0.001206	UGT2B15	UDP glucuronosyltransferase 2 family, polypeptide B15	46.69	2.92E-07	5.08E-04	UGT2B15	UDP glucuronosyltransferase 2 family, polypeptide B15	41.34	4.39E-08	0.000355	UGT2B15	UDP glucuronosyltransferase 2 family, polypeptide B15
2	40.23	1.12E-07	0.000949	UGT2B17	UDP glucuronosyltransferase 2 family, polypeptide B17	38.24	1.71E-07	4.81E-04	UGT2B17	UDP glucuronosyltransferase 2 family, polypeptide B17	31.38	2.14E-07	0.000534	UGT2B17	UDP glucuronosyltransferase 2 family, polypeptide B17
3	24.63	0.000015	0.003028	MIR21	microRNA 21	27.78	0.000004	1.10E-03	MIR21	microRNA 21	24.11	0.000018	0.002121	TNFSF10	tumor necrosis factor (ligand) superfamily, member 10
4	19.67	0.00003	0.003846	TNFSF10	tumor necrosis factor (ligand) superfamily, member 10	25.41	0.000018	1.77E-03	TNFSF10	tumor necrosis factor (ligand) superfamily, member 10	21.9	0.000079	0.004237	GDF15	growth differentiation factor 15
5	16.55	0.000161	0.008027	GDF15	growth differentiation factor 15	16.07	0.000002	3.41E-03	GDF15	growth differentiation factor 15	16.46	0.000001	0.000775	MIR21	microRNA 21
6	15.18	0.00007	0.001521	MSMB	microseminoprotein, beta-	15.63	0.000046	4.23E-04	CMAHP (non-coding)	cytidine monophospho-N-acetylneuraminic acid hydroxylase, pseudogene	16.24	8.50E-07	0.000534	MSMB	microseminoprotein, beta-
7	15.12	0.00009	0.000525	CMAHP (non-coding)	cytidine monophospho-N-acetylneuraminic acid hydroxylase, pseudogene	15.48	0.000078	5.88E-04	MSMB	microseminoprotein, beta-	15.86	2.97E-07	0.000601	CMAHP (non-coding)	cytidine monophospho-N-acetylneuraminic acid hydroxylase, pseudogene
8	13.48	6.64E-07	0.000496	CMAHP (coding)	cytidine monophospho-N-acetylneuraminic acid hydroxylase, pseudogene	14.39	5.02E-08	3.02E-04	CMAHP (coding)	cytidine monophospho-N-acetylneuraminic acid hydroxylase, pseudogene	15.25	0.000023	0.000534	CMAHP (coding)	cytidine monophospho-N-acetylneuraminic acid hydroxylase, pseudogene
9	11.78	3.21E-08	0.003542	LINC01087	long intergenic non-protein coding RNA 1087	13.88	5.14E-07	1.10E-03	TNFAIP3	tumor necrosis factor, alpha-induced protein 3	12.69	3.92E-07	0.002055	TNFAIP3	tumor necrosis factor, alpha-induced protein 3
10	11.38	0.00001	0.005684	TNFAIP3	tumor necrosis factor, alpha-induced protein 3	13.75	0.000023	0.003158	LINC01087	long intergenic non-protein coding RNA 1087	10.96	2.32E-07	0.001067	CAPN9	calpain 9

Compilation of top 10 up-regulated genes in 3D from results of microarray differential expression (DE) analysis. Significant DE up-regulated genes from triplicate samples of MCF-7 2D versus 3D condition (polyHEMA, ultra-low attachment or methylcellulose) were determined based on cutoff of ANOVA p value of <0.05 and a fold change greater than 2 fold. (pHEMA: 1809 DE, 942 up-regulated in 3D; ULA: 2117 DE, 904 up-regulated in 3D; mCELL: 1822 DE, 809 up-regulated in 3D)

Transcript cluster IDs that were not annotated with a gene symbol or containing _hap (haplotype chromosomes) were excluded from top-10 and were as follows: TC05000962.hg.1, TC02000102.hg.1, TC10002067.hg.1, TC4_ctg9_hap1000004.hg.1

Table 3

GAGE pathway analysis for top-10 perturbed pathways from monolayer to spheroid culture of MCF-7 cells.

	PolyHEMA		Ultra-low Attachment		Methylcellulose	
Rank	**Pathway**	**FDR p-value**	**Pathway**	**FDR p-value**	**Pathway**	**FDR p-value**
1	hsa04110 Cell cycle	1.40E-31	hsa04110 Cell cycle	1.74E-31	hsa04110 Cell cycle	9.33E-31
2	hsa03030 DNA replication	2.34E-22	hsa03030 DNA replication	4.08E-21	hsa03030 DNA replication	1.01E-20
3	hsa03013 RNA transport	1.39E-10	hsa03013 RNA transport	1.83E-11	hsa03460 Fanconi anemia pathway	2.12E-09
4	hsa00240 Pyrimidine metabolism	2.74E-10	hsa00240 Pyrimidine metabolism	3.85E-10	hsa03013 RNA transport	2.12E-09
5	hsa03460 Fanconi anemia pathway	3.86E-10	hsa03460 Fanconi anemia pathway	1.35E-09	hsa04068 FoxO signaling pathway	2.23E-09
6	hsa03040 Spliceosome	9.00E-10	hsa04068 FoxO signaling pathway	2.16E-09	hsa00240 Pyrimidine metabolism	2.96E-09
7	hsa04114 Oocyte meiosis	4.86E-09	hsa04114 Oocyte meiosis	1.80E-08	hsa04114 Oocyte meiosis	6.24E-08
8	hsa03430 Mismatch repair	7.32E-09	hsa03430 Mismatch repair	2.03E-08	hsa03430 Mismatch repair	6.24E-08
9	hsa04068 FoxO signaling pathway	2.17E-08	hsa03050 Proteasome	4.41E-08	hsa04115 p53 signaling pathway	2.09E-07
10	hsa04115 p53 signaling pathway	1.67E-07	hsa04115 p53 signaling pathway	6.36E-08	hsa03410 Base excision repair	5.53E-07

The transcript cluster ID from differential expression analysis with the highest average expression per gene in each dataset was selected to represent the expression of that gene. Significantly perturbed KEGG (Kyoto Encyclopedia of Genes and Genomes, [1]) pathways within each dataset were found using the Gene Set Analysis method Generally Applicable Gene-set Enrichment (GAGE). Top 10 pathways and corresponding q-value are displayed for each 3D condition.